AD-A042 362 STANFORD RESEARCH INST MENLO PARK CALIF F/G 18/6
DEVELOPMENT AND FABRICATION OF STRESS GAGES AND POWER SUPPLIES --ETC(U)
NOV 76 D D KEOUGH, D R CURRAN DNA001-75-C-0153
UNCLASSIFIED DNA-4236F NL

1 OF 1
ADA042362

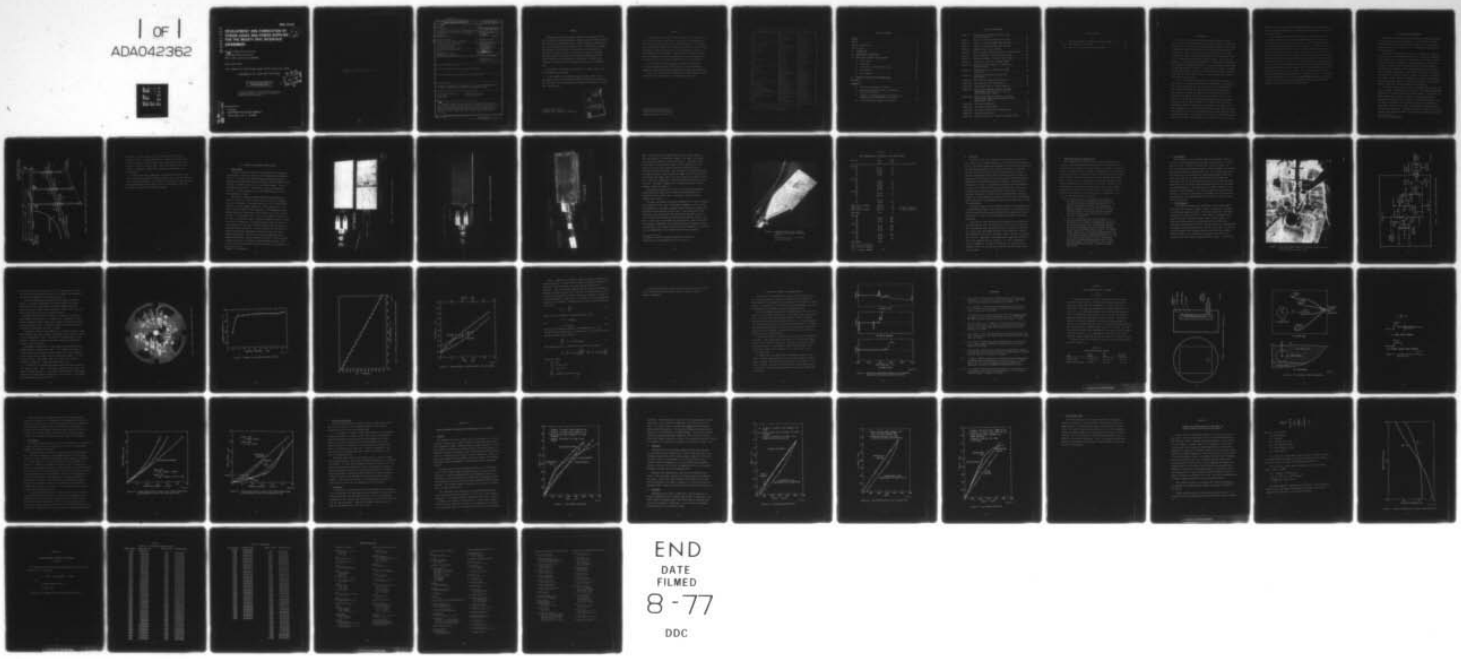

END
DATE FILMED
8-77
DDC

DNA 4236F

DEVELOPMENT AND FABRICATION OF STRESS GAGES AND POWER SUPPLIES FOR THE MIGHTY EPIC INTERFACE EXPERIMENT

Stanford Research Institute
333 Ravenswood Avenue
Menlo Park, California 94025

November 1976

Final Report for Period November 1974—November 1976

CONTRACT No. DNA 001-75-C-0153

APPROVED FOR PUBLIC RELEASE;
DISTRIBUTION UNLIMITED.

THIS WORK SPONSORED BY THE DEFENSE NUCLEAR AGENCY UNDER RDT&E RMSS CODES K400076462 J34DAXYX96902 AND K400076462 J34EAXYX96907 H2590D.

Prepared for
Director
DEFENSE NUCLEAR AGENCY
Washington, D. C. 20305

Destroy this report when it is no longer needed. Do not return to sender.

UNCLASSIFIED

SECURITY CLASSIFICATION OF THIS PAGE (When Data Entered)

REPORT DOCUMENTATION PAGE	READ INSTRUCTIONS BEFORE COMPLETING FORM
1. REPORT NUMBER: DNA 4236F	2. GOVT ACCESSION NO. / 3. RECIPIENT'S CATALOG NUMBER
4. TITLE (and Subtitle): DEVELOPMENT AND FABRICATION OF STRESS GAGES AND POWER SUPPLIES FOR THE MIGHTY EPIC INTERFACE EXPERIMENT	5. TYPE OF REPORT & PERIOD COVERED: Final Report for Period Nov 74—Nov 76
	6. PERFORMING ORG. REPORT NUMBER: SRI-PYU-3875
7. AUTHOR(s): Douglas D. Keough; Donald R. Curran, Project Supervisor	8. CONTRACT OR GRANT NUMBER(s): DNA 001-75-C-0153
9. PERFORMING ORGANIZATION NAME AND ADDRESS: Stanford Research Institute, 333 Ravenswood Avenue, Menlo Park, California 94025	10. PROGRAM ELEMENT, PROJECT, TASK AREA & WORK UNIT NUMBERS: NWET Subtasks J34DAXYX969-02 and J34EAXYX969-07
11. CONTROLLING OFFICE NAME AND ADDRESS: Director, Defense Nuclear Agency, Washington, D.C. 20305	12. REPORT DATE: November 1976
	13. NUMBER OF PAGES: 64
14. MONITORING AGENCY NAME & ADDRESS (if different from Controlling Office)	15. SECURITY CLASS (of this report): UNCLASSIFIED
	15a. DECLASSIFICATION/DOWNGRADING SCHEDULE

16. DISTRIBUTION STATEMENT (of this Report)

Approved for public release; distribution unlimited.

17. DISTRIBUTION STATEMENT (of the abstract entered in Block 20, if different from Report)

18. SUPPLEMENTARY NOTES

This work sponsored by the Defense Nuclear Agency under RDT&E RMSS Codes K400076462 J34DAXYX96902 and K400076462 J34EAXYX96907 H2590D.

19. KEY WORDS (Continue on reverse side if necessary and identify by block number)

Stress Gage Measurements
Ground Shock
Mighty Epic
Shielded Stress Gages
Gage Power Supplies

20. ABSTRACT (Continue on reverse side if necessary and identify by block number)

Shielded ytterbium stress gages and low current dc supplies were designed and tested for use with the Develco hardened telemetering canister. Gages, special double-shielded twinax cables and power supplies were constructed for the Mighty Epic interface experiment. Waterways Experiment Station (WES) fielded the stress systems, recorded and reduced the data.

DD FORM 1 JAN 73 1473 EDITION OF 1 NOV 65 IS OBSOLETE

UNCLASSIFIED

SECURITY CLASSIFICATION OF THIS PAGE (When Data Entered)

332-500

SUMMARY

Ytterbium stress gages and power supplies were developed for use with a hardened, remote data-handling system designed for DNA by Develco.* The system was used on Mighty Epic to record and transmit ground motion data in the region around a geological fault. Proximity of the ground motion sensors and orientation of the cables to the nuclear source dictated that gages and cables be modified by electrical shielding. Additional gages were constructed for Waterways Experiment Station (WES) to measure stress throughout the fault zone. Fielding, data recording, and reduction were performed by WES and are not presented here.

The design, construction, and testing of the gages, cables, and power supplies are described.

A brief summary of constraints on gage accuracy and an interpretation of data from the various geological regions of the interface are discussed. Gage calibration data, necessary for reduction of field data, are presented.

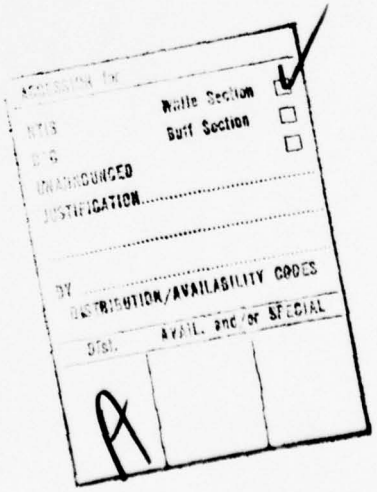

*Develco, Inc., Sunnyvale, California.

PREFACE

The Mighty Epic stress gage system represents the efforts of many of the staff of Poulter Laboratory. Specifically, John Hannigan was primarily responsible for the design and construction of the shielded gage configuration, and Ken Hirschberg and Lee Hall for the power supply and cables. Others contributing were William Wilkinson, Jim Yost, Frank Galimba, and William Murri; Noble Johnson* was project leader, Dr. Carl Petersen† was project supervisor for the initial portion of the project, and D. R. Curran was supervisor for the final phases.

Dr. Ray Shunk of Electro Mechanical Systems of New Mexico, Dr. Bruce Hartenbaum of RDA, and LTC Bruce H. Ellis and LCDR John Gallamore of DNA Field Command, coordinated the Mighty Epic Experiment.

Messrs. Don Day and Francis Haynes of Waterways Experiment Station conducted field installation, data recording and reduction.

---

*Currently with Xerox Corporation

†Currently with S^3, La Jolla, CA.

CONVERSION FACTORS FOR U.S. CUSTOMARY TO METRIC (SI) UNITS OF MEASUREMENT

To Convert From	To	Multiply By
angstrom	meters (m)	1.000 000 × E -10
atmosphere (normal)	kilo pascal (kPa)	1.013 25 × E +2
bar	kilo pascal (kPa)	1.000 000 × E +2
barn	meter^2 (m^2)	1.000 000 × E -28
British thermal unit (thermochemical)	joule (J)	1.054 350 × E +3
calorie (thermochemical)	joule (J)	4.184 000
cal (thermochemical)/cm^2	mega joule/m^2 (MJ/m^2)	4.184 000 × E -2
curie	giga becquerel (GBq)*	3.700 000 × E +1
degree (angle)	radian (rad)	1.745 329 × E -2
degree Fahrenheit	degree kelvin (K)	$t_k = (t°f + 459.67)/1.8$
electron volt	joule (J)	1.602 19 × E -19
erg	joule (J)	1.000 000 × E -7
erg second	watt (W)	1.000 000 × E -7
foot	meter (m)	3.048 000 × E -1
foot-pound-force	joule (J)	1.355 818
gallon (U.S. liquid)	meter^3 (m^3)	3.785 412 × E -3
inch	meter (m)	2.540 000 × E -2
jerk	joule (J)	1.000 000 × E +9
joule/kilogram (J/kg) (radiation dose absorbed)	Gray (Gy)	1.000 000
kilotons	*terajoules*	4.183
kip (1000 lbf)	newton (N)	4.448 222 × E +3
kip/inch^2 (ksi)	kilo pascal (kPa)	6.894 757 × E +3
ktap	newton-second/m^2 (N-s/m^2)	1.000 000 × E +2
micron	meter (m)	1.000 000 × E -6
mil	meter (m)	2.540 000 × E -5
mile (international)	meter (m)	1.609 344 × E +3
ounce	kilogram (kg)	2.834 952 × E -2
pound-force (lbf avoirdupois)	newton (N)	4.448 222
pound-force inch	newton-meter (N-m)	1.129 848 × E -1
pound-force inch	newton/meter (N/m)	1.751 268 × E +2
pound-force foot^2	kilo pascal (kPa)	4.788 026 × E -2
pound-force inch^2 (psi)	kilo pascal (kPa)	6.894 757
pound-mass (lbm avoirdupois)	kilogram (kg)	4.535 924 × E -1
pound-mass-foot^2 (moment of inertia)	kilogram-meter^2 (kg/m^2)	4.214 011 × E -2
pound-mass foot^3	kilogram/meter^3 (kg/m^3)	1.601 846 × E +1
rad (radiation dose absorbed)	Gray (Gy)+	1.000 000 × E -2
roentgen	coulomb/kilogram (C/kg)	2.579 760 × E -4
shake	second (s)	1.000 000 × E -8
slug	kilogram (kg)	1.459 390 × E +1
torr (mm Hg, 0°C)	kilo pascal (kPa)	1.333 22 × E -1

*The becquerel (Bq) is the SI unit of radioactivity; 1 Bq = 1 event/s.

+The Gray (Gy) is the SI unit of absorbed radiation.

TABLE OF CONTENTS

LIST OF ILLUSTRATIONS

LIST OF TABLES

I INTRODUCTION

Failure of electrical cables during ground shock has severely restricted UGT data and could limit deep basing concepts. Particularly vulnerable are regions of large local differential motion such as occur at geological faults and joints, and also large distributed relative motion such as occurs along cables lying in the plane of the shock. Techniques for cable hardening in those regions and alternative methods of data transmission are being investigated by DNA. One of the most promising of the transmission techniques is low-frequency electromagnetic (EM) propagation through the ground. A system using ground propagation is under development by Develco. In this system, a canister, hardened against ground shock, receives data from nearby hard-wired transducers, stores the data and transmits them to a remote station upon receipt of a command from that station.

To test the Develco canister and to obtain ground motion data in the vicinity of a geological interface, an experiment was conducted as part of the Mighty Epic UGT. The objectives of the work described in this report were to develop, construct, and test ytterbium gages, power supplies, and cables compatible with the Develco system and suitable for measuring free-field stress in the UGT. Late in the program, a task was added to construct additional gages, gage holders, and cables (but not power supplies) for a hardened canister system developed by Waterways Experiment Station (WES). The purpose of the WES measurement was to obtain free-field ground motion above and below the geological interface, the measurements below being redundant to the Develco measurement. The gage and cable designs for the WES measurements were therefore essentially identical to the Develco system. The power

supplies for the WES gages were designed and constructed by WES and were a version of those developed at SRI, modified to permit preshot calibration of the gage system.

Field installation of the Develco canister was accomplished by WES and Develco. Installation of the WES hardened canisters and recording and reduction of data were performed by WES. Details of these activities are presented in separate reports by those agencies. We have included a brief description of the experimental layout to illustrate unusual gage and cable design requirements, and have briefly described the field test results for completeness. The principal material presented in the following sections, however, describes the design, construction, and testing of the gages, power supplies, and cables. It will be noted that two configurations of shielded stress gages (paddle and cylindrical) are described, although only the paddle gage was used in Mighty Epic. The cylindrical gage evolved during the program when it was thought that the Develco system would be fielded on Husky Pup, which required the cylindrical geometry. We include its description because the laboratory shock-loading tests of the shielded grid for both types of gages were performed on this configuration and because this gage may be useful in future tests.

II EXPERIMENTAL REQUIREMENTS

The physical configuration of the Mighty Epic interface experiment was sufficiently different from prior free-field layouts to require redesign of the gages, cables, and power supplies. To better understand the nature of the revisions, it is instructive to describe the configuration here.

In a typical* arrangement, the gage is positioned in a long hole drilled radial to the working point (WP) or in a short hole tangential to the shock front. In both cases the length of cable close to the WP is kept to a minimum to reduce the induced electrical signals and to reduce the length of cable subjected to high stress shock loading. In addition, power supplies and recording equipment are well removed from the ground shock region. Being remote, with access to ac power, the supplies can provide sufficient current to the gages to ensure that data signals will be well above induced noise without extra shielding of gages and cables. This is a significant advantage since shielding greatly complicates both construction and installation.

By contrast to the "typical" system, the Mighty Epic configuration, shown in Figure 1, resulted in long lengths of cable running essentially tangential to the ground shock and in high EM fields. In addition, the power supplies were located in canisters within the ground shock environment (Develco system), as shown, and required mechanical as well as electrical hardening. In the Develco system, data recording was performed in the canister as well, which therefore required batteries to assure post-shock power. Because of the battery power, gage viewing currents were necessarily lower. This reduction, coupled with the close

*UGT free-field measurement.

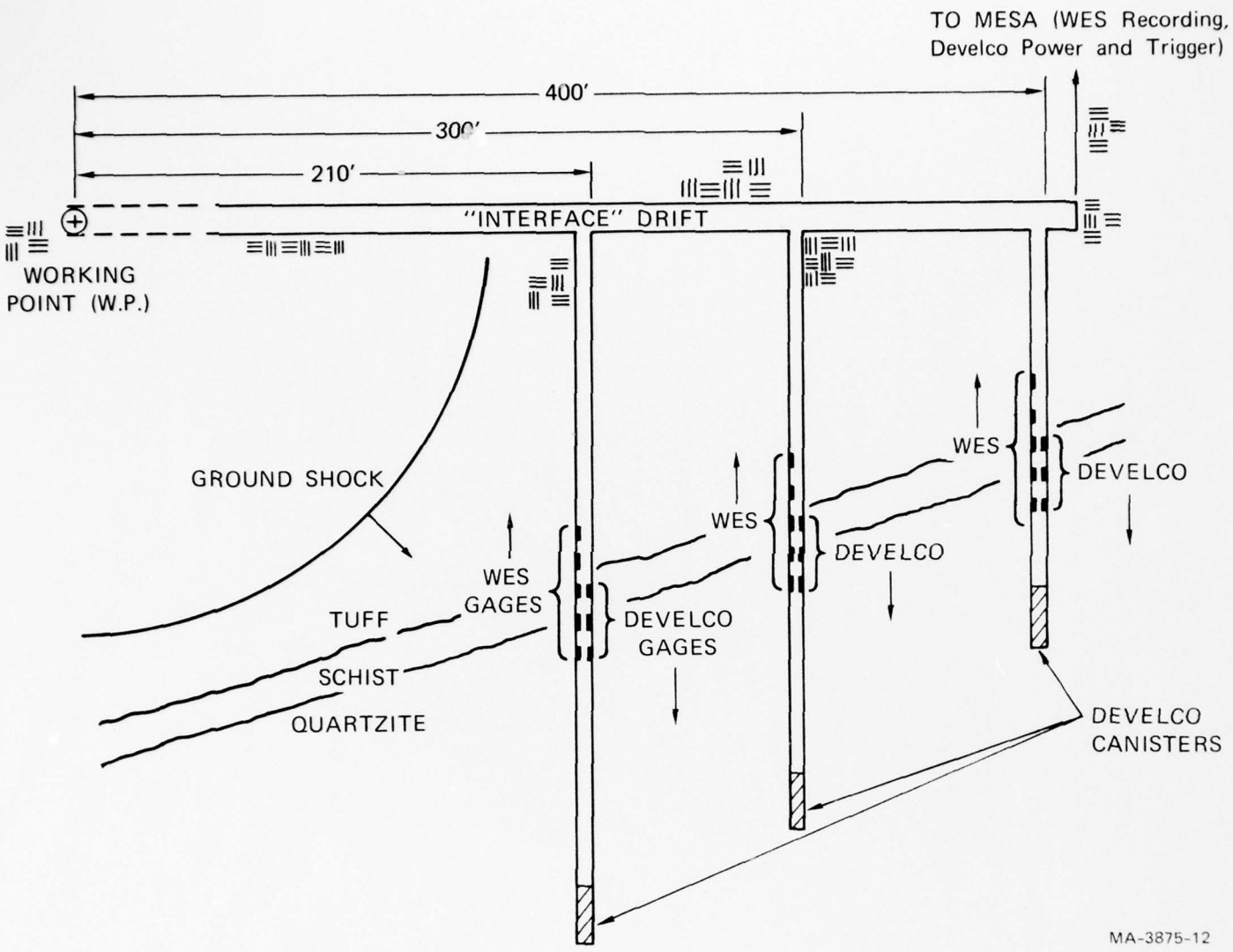

FIGURE 1 ELEVATION VIEW OF STRESS GAGE LAYOUT FOR INTERFACE EXPERIMENT

proximity to the WP mandated the use of shielded gages and doubly shielded cables. To further decrease the probability of electrical pickup, a balanced circuit system was used that utilized twinax cable in place of the usual coaxial cable. These requirements could not be found in a commercial, rugged cable and necessitated special cable construction.

In addition to these requirements, the gages had to record "free-field" stress in the widely different geological media, tuff and quartzite, of the interface experiment. The effect of the two media on the measurement presented additional problems of data interpretation. These are discussed in detail in the following sections.

III MIGHTY EPIC INTERFACE STRESS SYSTEM

A. Stress Gages

The basic concepts. calibration, and testing of the ytterbium piezoresistant, soil-stress gage have been abundantly described elsewhere.[1-6] We present here primarily design modifications made to incorporate shielding and structural strength into the "paddle" configuration, and shock loading tests of these modifications. We have included brief summaries of constraints on gage calibration and validity of stress measurement to aid in interpretation of field data (Appendices A and B).

The shielded, paddle gage design developed for Mighty Epic is shown in Figures 2, 3, and 4, which illustrate the basic components and stages of assembly. The gage consists of a 50 Ω, ytterbium grid bonded to a Kapton* backing (Figure 2). The ytterbium foil is the stress sensitive element of the transducer. The transducing element changes resistance proportional to the tensor state of strain within the foil.[4] The foil grid is 3 in. by 3 in. by 0.002 in. thick (50 Ω) or 0.001 in. thick (100 Ω gage). The grid elements are 0.015 in. wide with 0.015 in. separation. Electrical contact between the grid and inner conductors of the cable is made by braided leads configured in a serpentine pattern (Figure 2). Both the braid and pattern allow for possible differential displacements between grid and cable due to shock-induced motion. The grids and leads are sandwiched between copper clad fiberglass boards (commerical PC boards, 0.060 in. thick) as shown in Figure 3. Structural strength between the inner shield of the cable and the fiberglass boards, and electrical shielding at the

*Kapton, E. I. Du Pont Co.

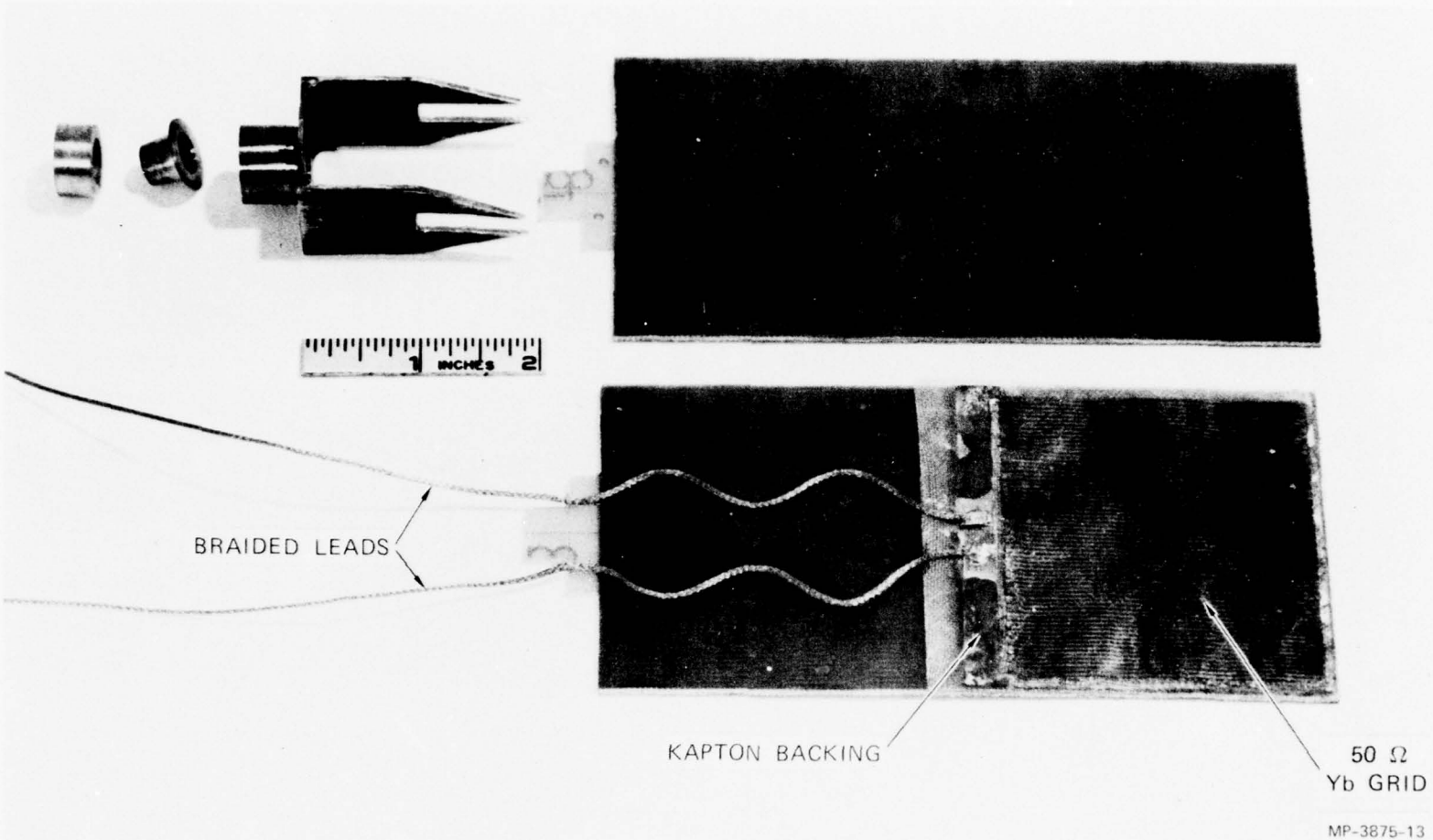

FIGURE 2 STAGE 1 OF YTTERBIUM PADDLE GAGE ASSEMBLY

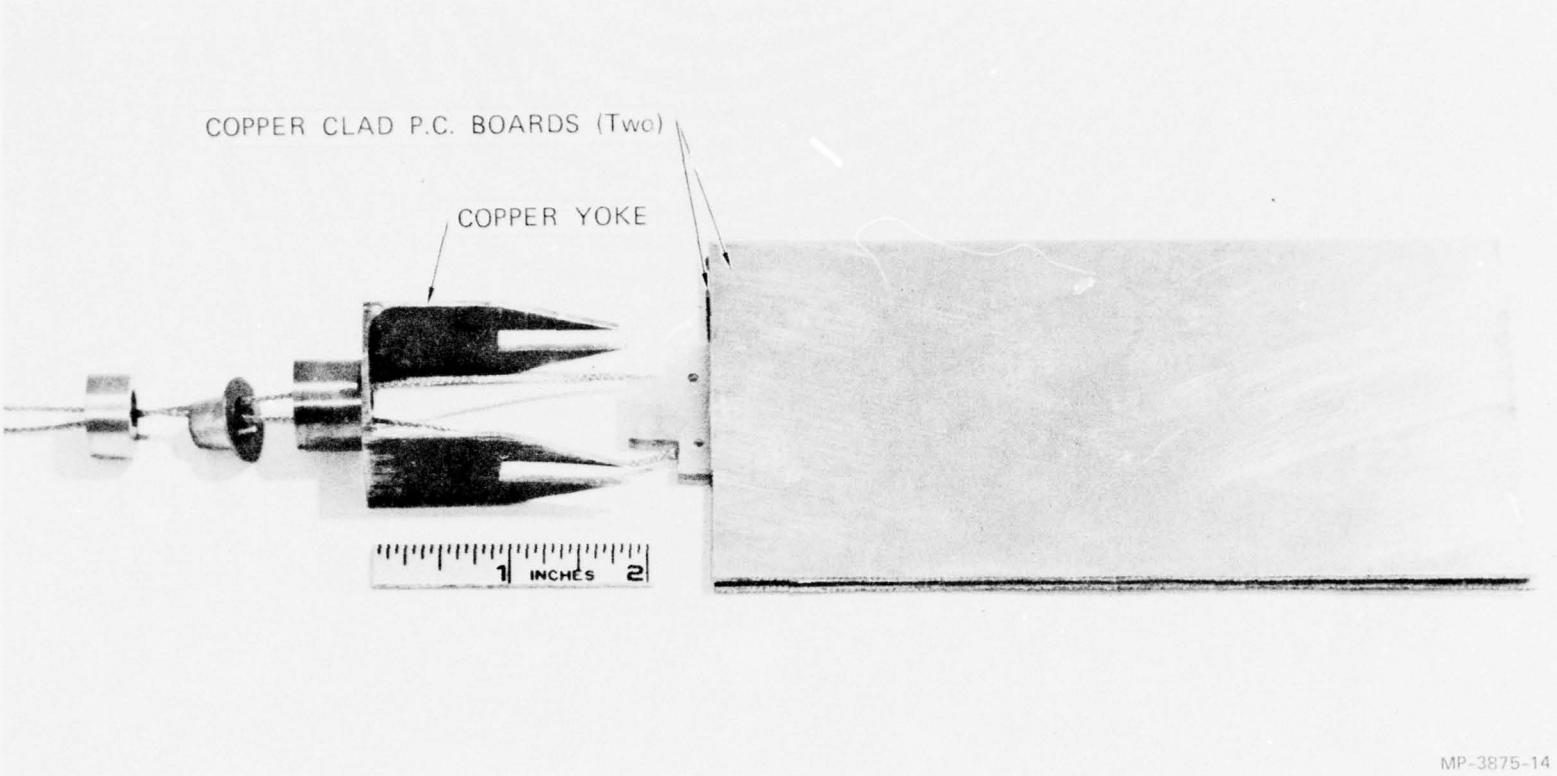

FIGURE 3 STAGE 2 OF YTTERBIUM PADDLE GAGE ASSEMBLY

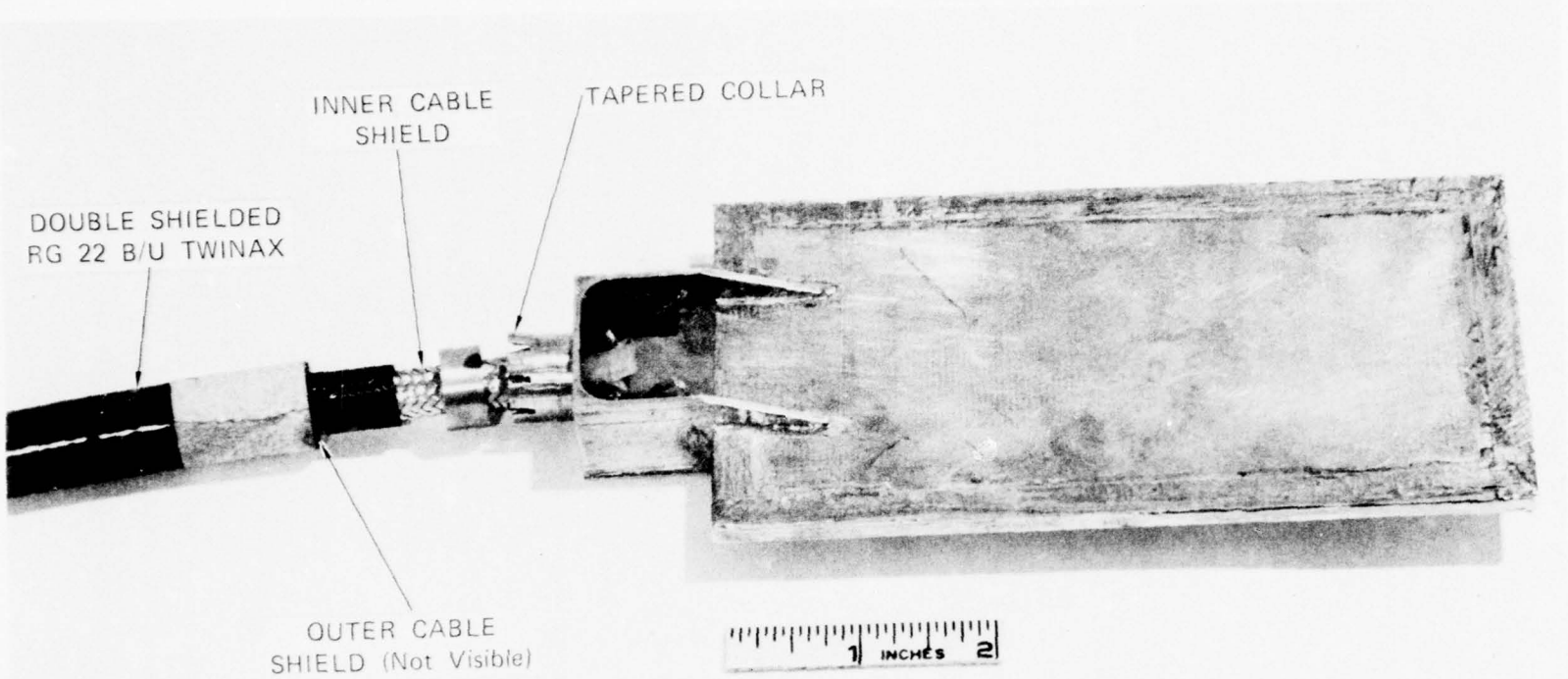

FIGURE 4 STAGE 3 OF YTTERBIUM PADDLE GAGE ASSEMBLY

gage are obtained from the copper yoke system, as shown (Figure 3). This inner shield is soldered and clamped to the yoke by the tapered plug and collar (shown most clearly in Figure 4). The outer shield of the twinax is cut back and allowed to float (electrically) with respect to the gage (the complete electrical shielding system is described in the next section). Gage shielding is completed by joining the copper cladding of the PC board with copper foil and covering the yoke opening with copper sheet. The inner volume of the yoke is potted with a low shear strength gel* to allow relative motion between the foil and leads. The gage is completed by an insulating coating of epoxy Homalite as shown in Figure 5.

The double-shielded RG22 B/U cable† was constructed by adding a second shield and insulation of abrasion resistant propylene to standard RG 22 B/U twinax cable. The cable is shown in the gage assembly view, Figure 4.

Ten gages with nominal electrical impedance of 50 Ω were constructed for the Develco system, and 17 with nominal impedance of 100 Ω for the WES measurements. The higher impedance gages represented a modification introduced to obtain higher signal levels. Gage nomenclature, grid resistances, and cable lengths for both systems are given in Table 1. It can be seen that the Develco cables were substantially longer (50 to 290 ft. versus 10 ft.) than those of the WES system. These long cables were primarily responsible for the double shielding requirement because the magnitude of the signal induced on the inner conductors of a shielded cable is proportional to the length for given field strengths.

---

*Cyanogum 41, American Cyanamid Company, Pearl River, NY.

†Manufactured by Storm Products, Inc., Palo Alto, CA.

FIGURE 5 COMPLETED PADDLE GAGE ASSEMBLY (COURTESY OF WATERWAYS EXPERIMENT STATION)

(Clamp and wire are part of a preshot EMP test performed by WES)

Table 1

GAGE NOMENCLATURE, RESISTANCES, AND CABLE LENGTHS

Yb Gage	Resis (Ω)	Cable (ft)	
WES 210			
W1	100.30	10	
W2	101.50	10	
W3	94.00	10	
W4	97.00	10	
*			
WES 300			
W1	93.84	10	
W2	94.42	10	
W3	86.04	10	
W4	92.26	10	
W5	93.04	10	
WES 400			
W1	103.38	10	
W2	101.74	10	
†			
W4	95.14	10	
W5	92.96	10	
WES A (Use as 210W5)	98.8	10	
WES B Spare	115.3	10	Has Lucite spacers
WES C (Use as 400W3)	107.5	10	at cable connection
WES SPARE	82.0	10	
DEV 210			
D3	55.54	290	
D4	53.09	270	
D5	54.12	250	
DEV 300			
D3	56.31	250	
D4	53.65	230	
D5	51.72	210	
DEV 400			
D3	49.88	100	
D4	53.33	75	
D5	44.19	50	
DEV SPARE	50.50	-	

*W5 - Use WES A (SPARE)

†W3 - Use WES C (SPARE)

B. Gage Tests

Two types of tests were performed, quality control tests of the grid elements, and a shock loading test of the grid and shield configuration. The quality checks were conducted on each grid by subjecting the ytterbium-Kapton assembles first to pulse excitation of 3 amps and 100 volts and second to dc (10 min) current excitation of 100 mA. Repeated, high-current pulsing tends to stabilize grid resistance by fusing poor joints between the foil and leads and also by eliminating possible hair-line bridges between grid elements. DC excitation is performed at a current of approximately 50% higher than that expected in field use to simulate worst case heating conditions. By using a constant current source and observing the voltage across the grid, resistance changes due to joule heating can be monitored. Excessive changes (not a major problem in pulse current excitation and recording) cause saturation of the recording circuits in the systems and are therefore unacceptable.

The pulse and dc tests were conducted prior to final bonding of the ytterbium-Kapton package to the fiberglass board. An additional pulse test was performed after encapsulation and before connecting the grid to the cable. A final test of continuity was performed after cable connection.

The effect of shock loading on the shielded grid was examined in one high explosive test. At the time of the test it was anticipated that a cylindrical gage configuration would be required for placement in a radial drill hole (Husky Pup Event) and therefore the armored grid assembly was cast into a cylinder of epoxy. However, the results are felt to be applicable to the Mighty Epic paddle gage because the basic grid configurations are identical. The test is described in detail in Appendix A. Results indicated that the armoring did not adversely effect the gage response within the pressure range tested, up to 3.4 kbar.

C. Constraints on Data Interpretation

The credibility of "free-field" stress data is dependent on the accuracy of data recording and reduction and also on the validity of the calibration functions by which gage output is reduced to free-field stress. Techniques for data recording and reduction are well developed.[7] Relating gage output to free-field stress is difficult in stress ranges where material strengths alter the local stress distributions around gages. In the case of the Mighty Epic measurements, the applicability of gage calibration data and the effect of the grout strength on the measurements in the different geological media were largely unknown. Bounds on the magnitude of the uncertainties in measurements from calibration and placement are reviewed briefly in Appendices B and C. It can be concluded from the review that:

- With respect to gage calibration, an uncertainty of not more than ±15% is introduced in the reduction of field data by using the calibration obtained for 1-D, planar, shock-loaded ytterbium. This uncertainty appears to apply over the range for which multiple loading path data exist, namely, 2 kbar. The shock data can therefore be used to reduce field records. These data, from an unpublished work of Ginsberg, are given in Appendix D.
- There is a pronounced effect of gage/grout/soil relative material strengths on gage response. Based on static, elastic analysis (referenced in Appendix C), the thickness-to-width ratio of the paddle configuration is sufficiently small that the gage registers stress in the surrounding grout to within a few percent. However, the stress in the grout column may be as much as 75% lower than that in a higher modulus medium, such as the granite below the Mighty Epic interface. In the tuff, above the interface, the moduli are probably sufficiently matched between grout and soil so that the gage registers free-field stress. This analysis does not include rate effects or changes in moduli with stress.

D. Gage Holders

The constraints on data interpretation discussed above apply to a more or less idealized emplacement of gages in drill holes. In reality, the hole is also a vehicle for experiments, canisters, cables, etc. that can be grossly mismatched in modulus. These inclusions also distort and alter the stress in and around the gage. In the Mighty Epic holes the WES canisters were connected by thick-walled tubing to which the gages were attached. To reduce possible distortion, holders were constructed that located the gages in the holes at as large a distance as possible from the tubing and maintained the plane of the grid normal to the shock direction. The holder design is shown in Figure 6. The completed assembly clamps to the canister connecting tubes and holds two gages. One gage was connected to the nearest (10 ft) WES canister and the other to the Develco canister at the bottom of the drill hole (from 80 to 400 ft.).

E. Power Supplies

As discussed previously, the requirements for the power supply were that it be low power, constant current, triggerable, and capable of withstanding mechanical shock. The circuit developed to meet these requirements is shown in Figure 7. Gage current is triggered by the optical isolators to decouple trigger cables from the supply. The shunt diode string protects the isolators from line transients. Switching is provided by the 2N 3643. Current regulation is accomplished by feedback from the Darlington pair, 2N 3143 and 2N 5194. The two 47-Ω resistors parallel with the gage terminate the twinax cable (double shielded RG22U) in its characteristic impedance and also form a balanced system that reduces common mode noise signals. The shunting

FIGURE 6 GAGES AND HOLDER MOUNTED ON CANISTER CONNECTING TUBE
(Courtesy of Waterways Experiment Station)

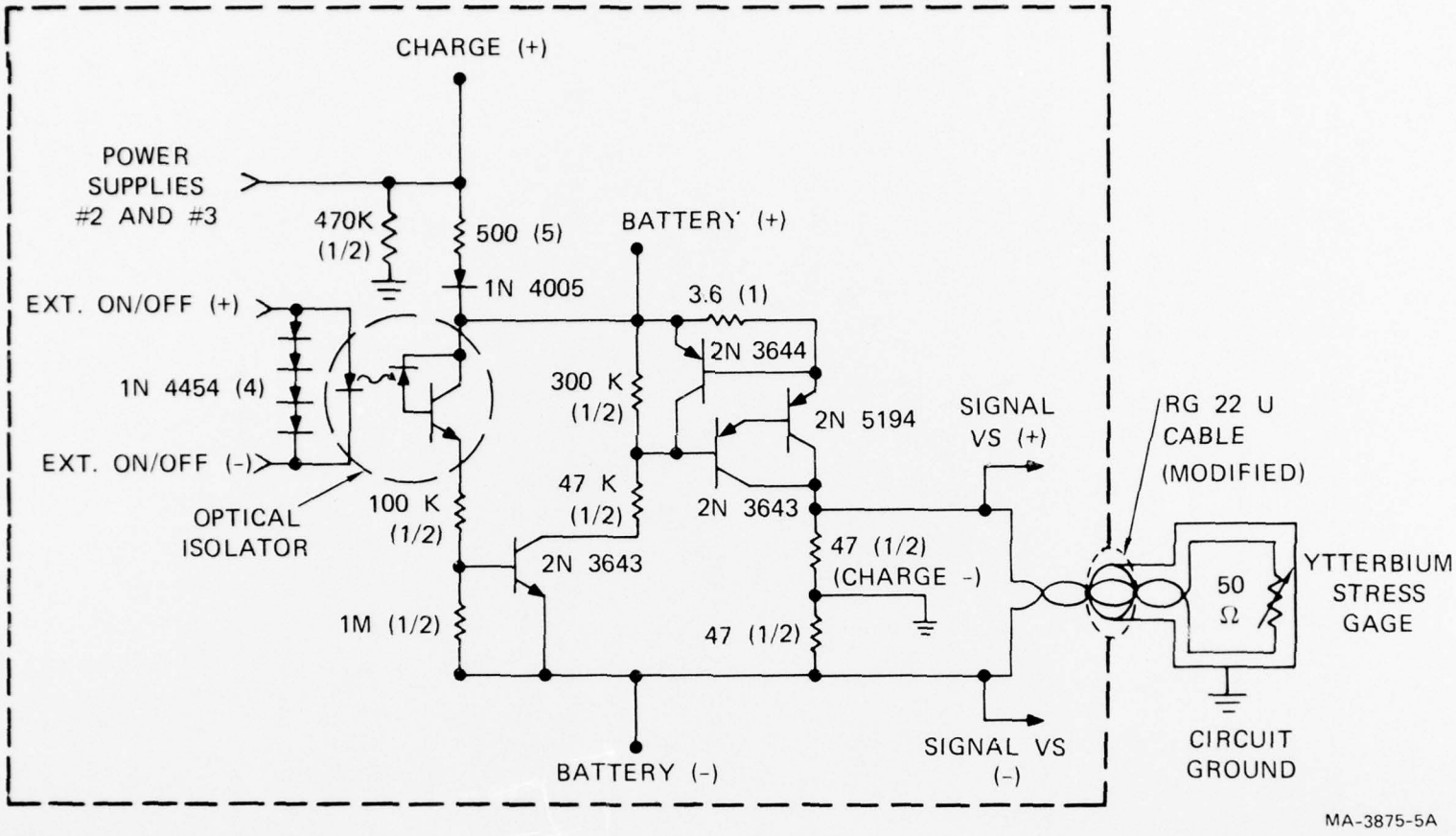

FIGURE 7 CIRCUIT DIAGRAM OF CONSTANT CURRENT SUPPLY

resistors reduce the gage sensitivity by $\sim 1/2$, however, it was felt that the noise rejection was necessary in the expected EMP environment and more than compensated for the reduced signals.

Electrical shielding of the gage and power supply are shown in Figure 7. The gage is connected to the inner shield of the twinax cable, which is also power supply local ground (negative battery). The outer shield is tied to canister ground, as shown. In essence, the entire supply and cable system is double shielded.

Battery charging current is limited to a maximum of 2 mA and is diode coupled to the circuit. The charge input is connected to local ground to suppress induced signals on the charge line should this line open during ground shock. Two identical constant current circuits for two gages are connected in parallel, as shown.

The physical layout of the supplies is as shown in Figure 8. Each board contains three power supplies and connects to the canister circuits via the circumferential holes. The boards are stacked axially in the canister. (Details of canister design and testing are presented in a separate report by Develco.)

Performance characteristics of the supply are illustrated by the response curves of Figures 9, 10, and 11. In Figure 9, the effect of battery voltage on the supply current is shown. The current indicated is that in the shunt resistors (two 47-Ω resistors, Figure 7). It can be seen that over a wide range, from 7 to 15 volts, the current is constant to within $\pm 2\%$. Normal operating level is 12v.

In Figure 10, the variation in supply current with gage resistance (50 Ω gage) is shown. Over a wide range of resistance, 45% change, the current decreases by only 11%. The expected maximum change in resistance expected in the Mighty Epic experiment was $\sim 22\%$ (3 kbar). Gage current would therefore be constant to with $\sim 6\%$.

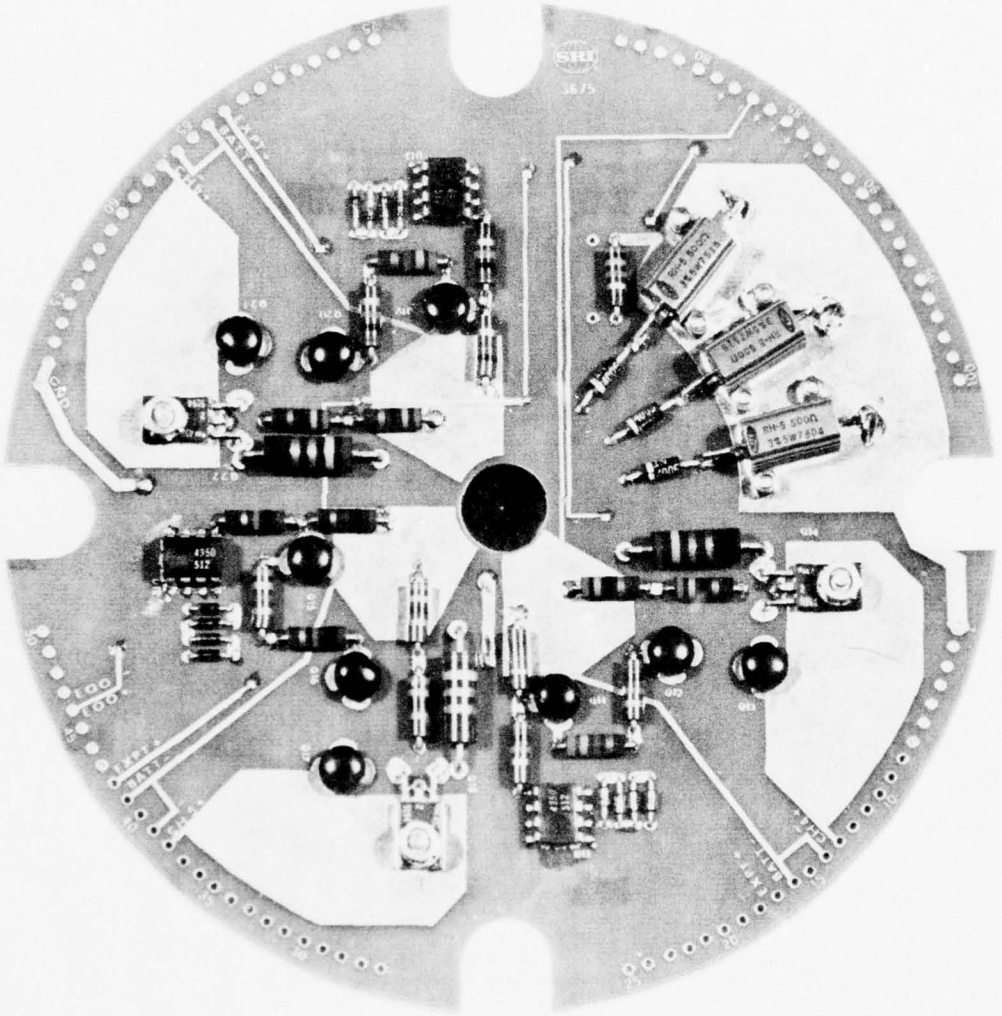

FIGURE 8 PHYSICAL ASSEMBLY OF CONSTANT CURRENT SUPPLY

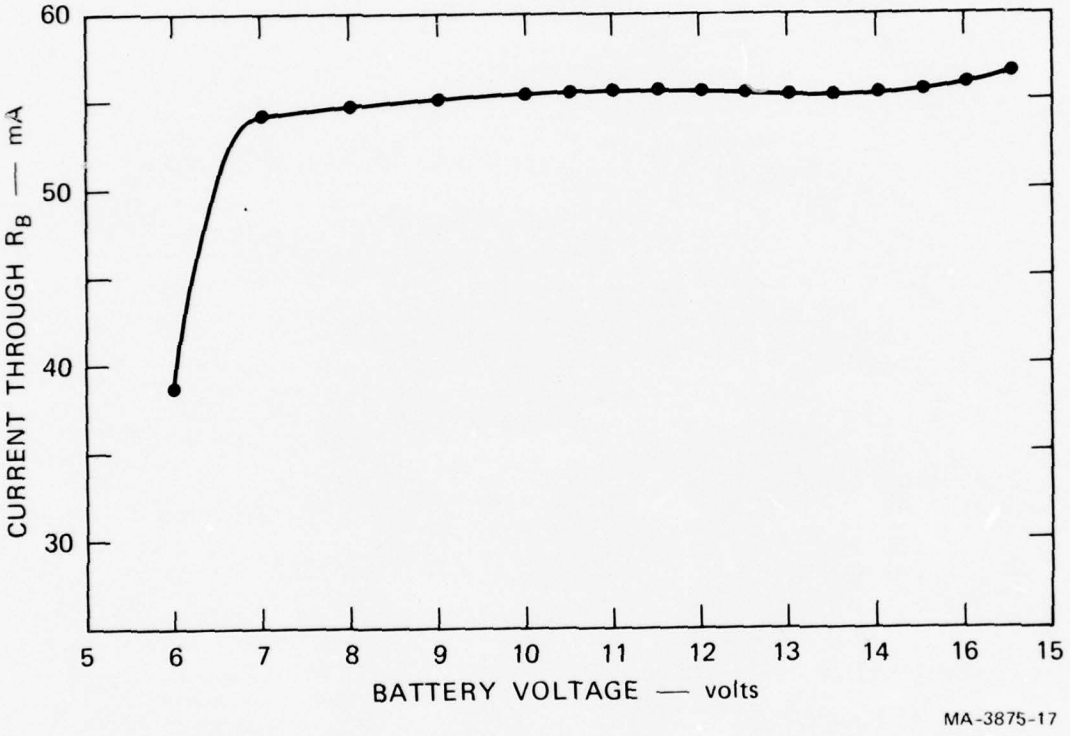

FIGURE 9 CURRENT AS A FUNCTION OF SUPPLY VOLTAGE

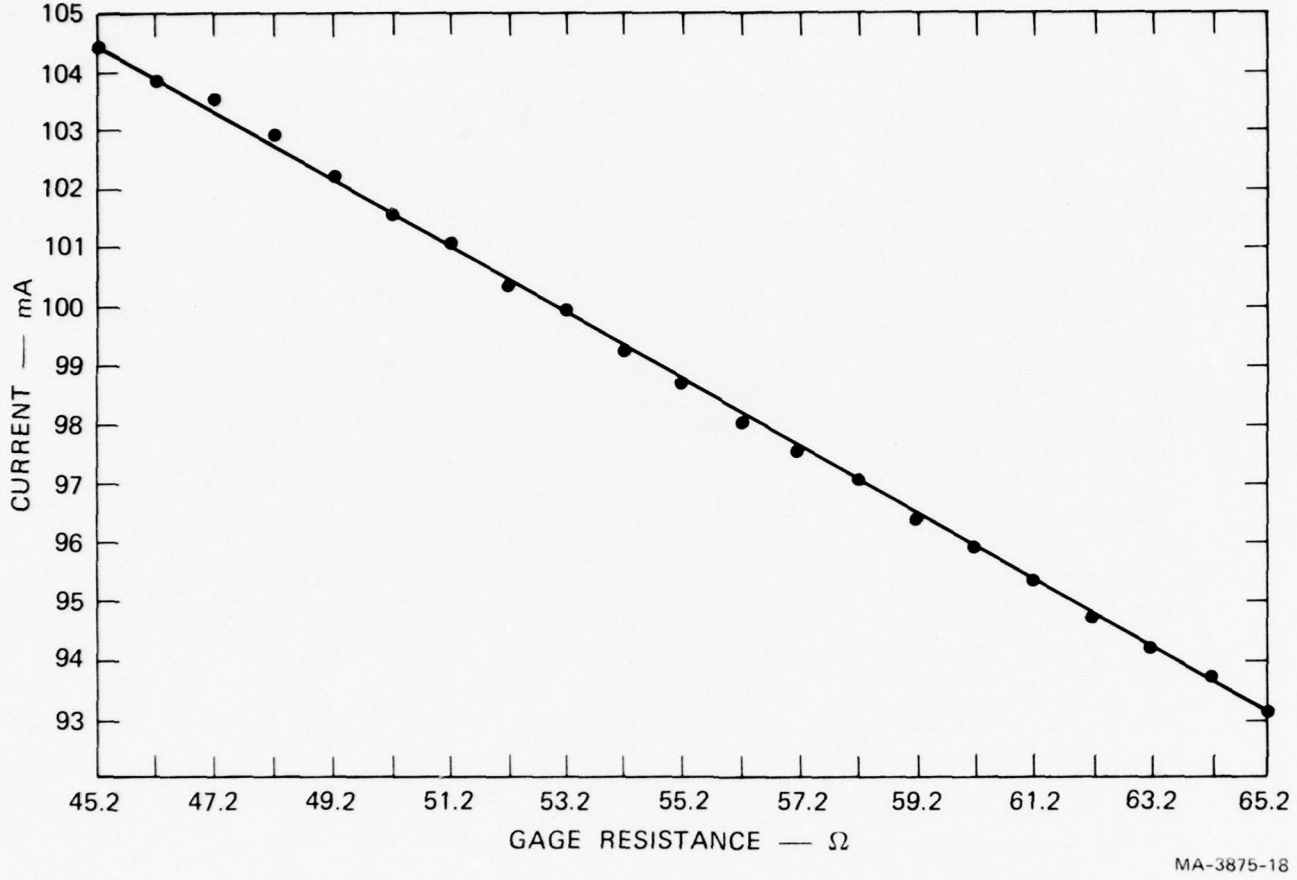

FIGURE 10 VARIATION IN GAGE CURRENT AS A FUNCTION OF GAGE RESISTANCE

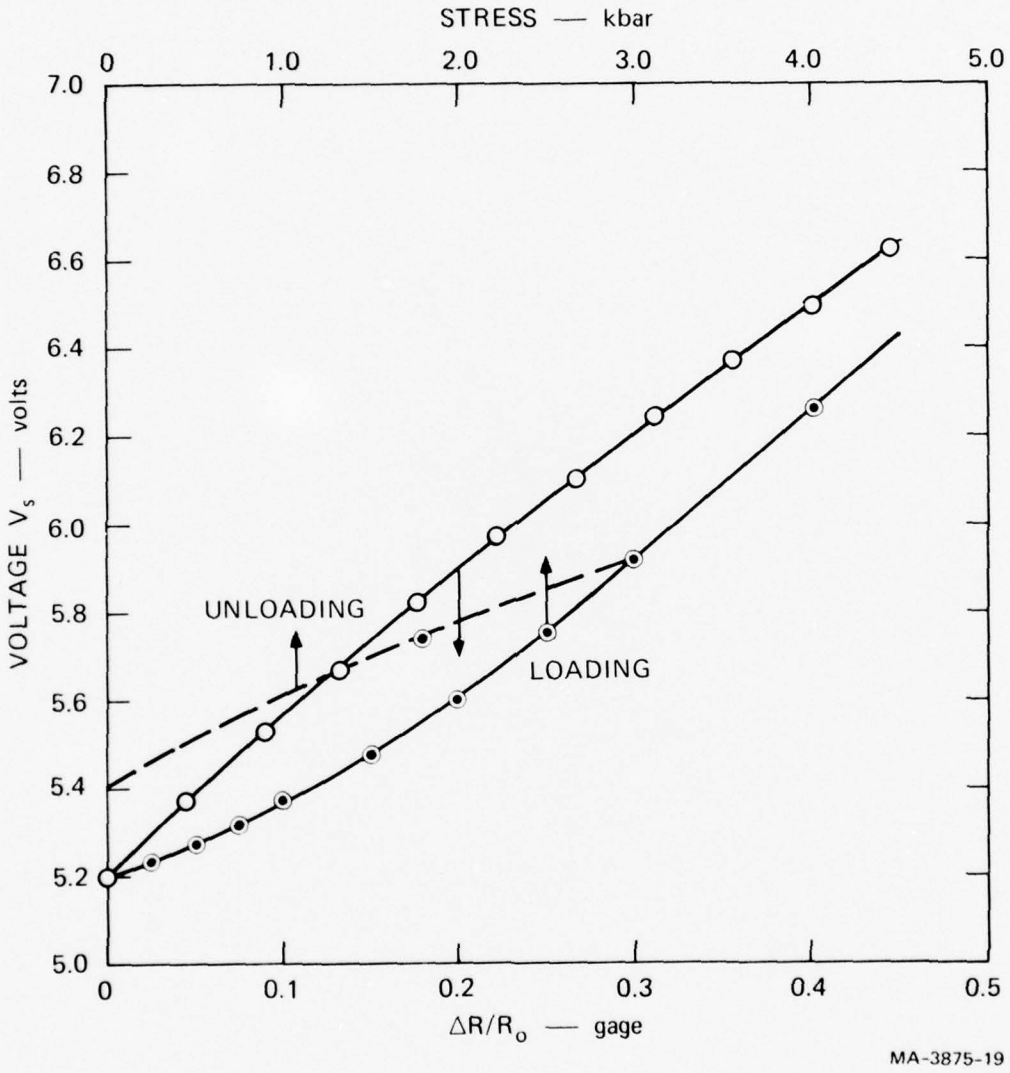

FIGURE 11 SIGNAL VOLTAGE V_s AS FUNCTIONS OF $\Delta R/R_o$ AND STRESS

Figure 11 shows the net effect of shunt resistance and current drop on gage sensitivity. Voltage across the gage is plotted as functions of resistance change and stress, the latter derived from the data of Appendix D. The curve labeled "loading" can also be used for unloading response from peak stresses up to ~ 1.1 kbar; the unload voltage reflects the hysteresis observed in ytterbium and must be converted to stress by a function dependent on peak stress. This function can be obtained from previous data as follows. Unloading data have been fitted by Ginsberg[4] to the form

$$\sigma_u = A + B\frac{\Delta R_u}{R_o} \tag{1}$$

where A and B are constants that depend on peak stress;

$$B = K_1 - K_2\,\sigma_{peak} \tag{2}$$

and

$$A = -\,B\,\Delta R_H/R_o \tag{3}$$

where R_H is the residual resistance in unloading, and R_o is the initial prestressed resistance. In Reference 4, the residual resistance has been related to peak stress by

$$\frac{\Delta R_H}{R_o} = -\,K_3 + K_4 \log_e \sigma_{peak}. \tag{4}$$

The unloading stress as a function of peak stress is therefore:

$$\sigma_u = \left(K_1 - K_2\,\sigma_{peak}\right)\left[\frac{\Delta R_u}{R_o} - \left(K_3 + K_4 \log_e \sigma_{peak}\right)\right] \tag{5}$$

where $K_1 = 24.26$

$K_2 = 1.81$

$K_3 = -\,6.87 \times 15^{-3}$

$K_4 = 5.42 \times 10^{-2}$

$\frac{\Delta R_u}{R_o}$ = unloading resistance change.

A sample unloading curve derived from the stress-resistance funtion of Eq. (5) and the resistance-voltage curve is shown in Figure 11 (labeled "unloading").

IV SUMMARY OF RESULTS AND RECOMMENDATIONS

In Section I it was noted that the scope of the SRI program did not include fielding, data recording, reduction and interpretation. These aspects of the experiment are presented by WES in separate reports. However, for completeness, we present here some preliminary test results and conclusions on adequacy of the stress measuring system.

Of the one Develco canister that returned partial data, the stress channels did not produce usable data. In the WES system, approximately 50% of the stress-MUX systems produced records. Three of the more significant records are shown in Figures 12, a, b, c. These represent data from tuff and quartzite of Hole #3 and tuff of Hole #4. In general, the amplitudes and arrival times are about as predicted. The failure times of the stress channels correspond to the loss of all data from the MUX's in the interface region.

Of particular note is the generally low noise level including zero time EMP. Since gage currents were only 50 ma, the excellent signal to noise ratio indicates that system shielding and signal processing were very effective. In particular, records from the gage in tuff (Figure 12c) clearly show a precursor of $\sim 7\%$ and a noise level of $< 2\%$ of peak stress.

It appears that the combination of shielding, constant current source, balanced twinax and MUX can yield a high resolution, credible stress measuring system that could be used over a wide range of soil stress. However, improving system reliability and defining gage-soil interaction at low stress levels remain two areas where further work is required.

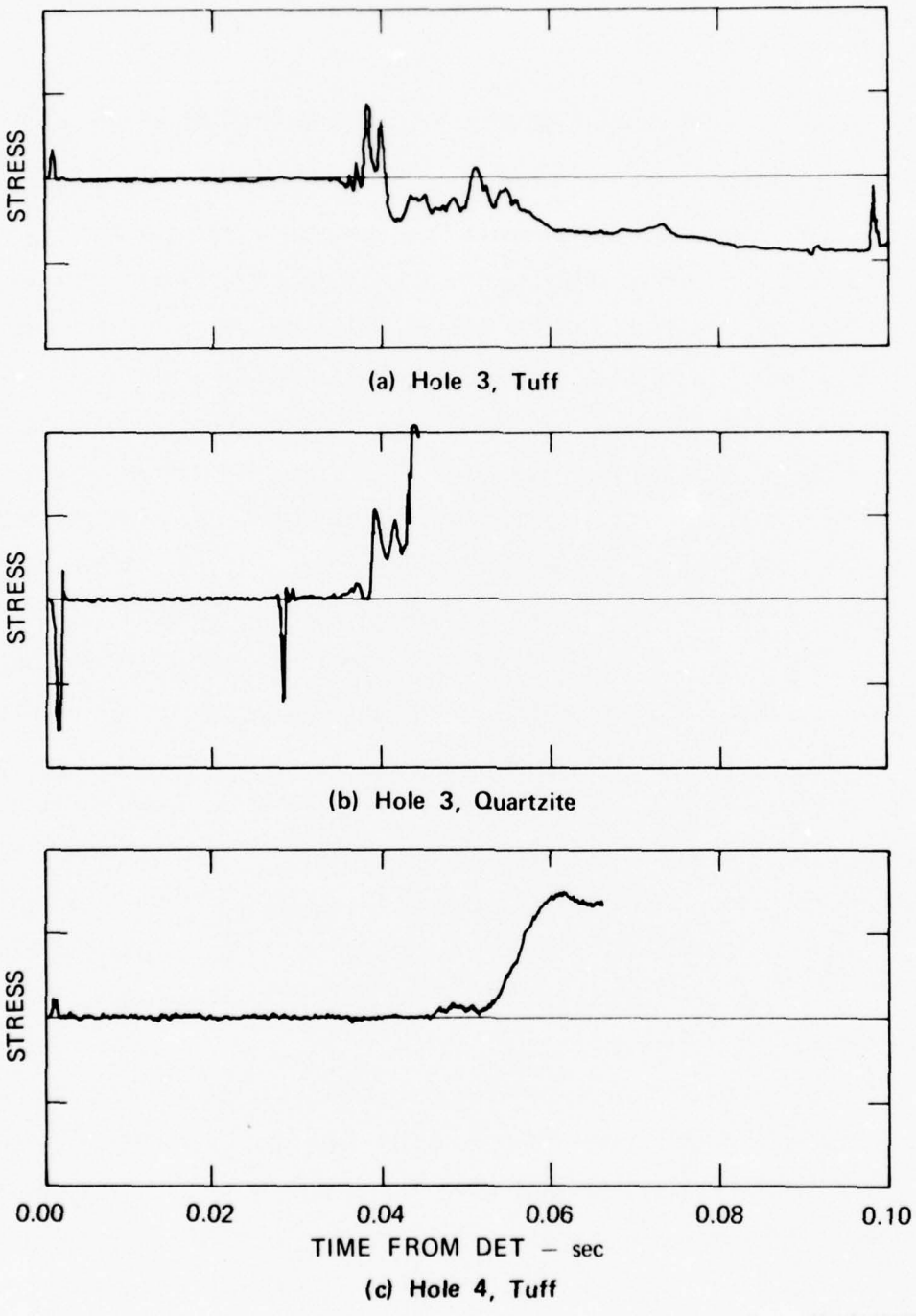

FIGURE 12 MIGHTY EPIC STRESS-TIME RECORDS, WES MEASUREMENTS (COURTESY OF WATERWAYS EXPERIMENT STATION)

REFERENCES

1. D. D. Keough, "Development of a High-Sensitivity Piezoresistive Transducer for the Low Kilobar Range," Final Report, DASA 2508, Stanford Research Institute, Menlo Park, CA (1970).

2. M. J. Ginsberg, "Calibration and Characterization of Ytterbium Stress Transducers," Final Report, DNA 2742F, Stanford Research Institute, Menlo Park, CA (1971).

3. C. W. Smith, et al., "Constitutive Relations from In Situ Lagrangian Measurements of Stress and Particle Velocity," Final Report, DNA 28031, Stanford Research Institute, Menlo Park, CA (1972).

4. M. J. Ginsberg, et al., "Effects of Stress on the Electrical Resistance of Ytterbium and Calibration of Ytterbium Stress Transducers," Final Report, DNA 3577F, Stanford Research Institute, Menlo Park, CA (1973).

5. C. W. Smith, et al., "In Situ Constitutive Relations of Soils and Rocks," Final Report, DNA 3678F, Stanford Research Institute, Menlo Park, CA (1974).

6. C. W. Smith, "Ytterbium Stress Gage Measurements at the Hard Pan Site," Topical Report, DNA 3805T, Stanford Research Institute, Menlo Park, CA (1975).

7. D. D. Keough, "Procedure for Fabrication and Operation of Manganin Shock Pressure Gages," Technical Report No. AFWL-TR-68-57, Stanford Research Institute, Menlo Park, CA (1966).

A-1. N. Froula, "Hugoniot Equation of State and Stress Wave Propagation in Saturated Ottawa Banding Sand at +20°C and -10°C," S^3 Final Report for U. S. Army Cold Regions Research and Engineering Laboratory, Contract No. DACA89-81-C-0026 (September 1971).

C-1. D. W. Taylor, "Pressure Distribution Theories, Earth Pressure Coil Investigations and Pressure Distribution Data," U. S. Waterways Exponent Station, Vicksburg, MI (1947).

Appendix A

TEST OF SHIELDED GAGE, 3 KILOBARS

By
W. J. Murri

To investigate possible effects of electrical shields on gage mechanical shock response, a shielded gage in epoxy and standard fiberglass paddle gages were subjected to a 3 kbar stress wave in a sand medium. The epoxy gage configuration is shown schematically in Figure A-1. The vulnerable region of the double-shielded design was felt to be around the cable-to-grid joints. The test was conducted primarily to determine the behavior in these regions. The pressure source of 121 lbs of nitromethane and the gage layout are shown in Figure A-2. The gages were 18 ± 1/8 in. from the high explosive surface and were located at an expected peak stress of 2 to 3 kbar. The sand was sprayed with water after emplacement of the gages and until puddles formed on the surface. It was thought that near-saturation could be obtained; however, apparently this was not achieved, as discussed below.

Results of the test are shown in Table A-1 and in the voltage-time traces of Figure A-3.

Table A-1

HIGH EXPLOSIVE TEST RESULTS

Gage	Peak Stress	Rise Time	Recording Duration
Paddle gages	2 kbar (Av.)	18 μsec (Av.)	< 100 μsec
Homalite block gage	~3.4 kbar	17 μ sec	> 500 μsec

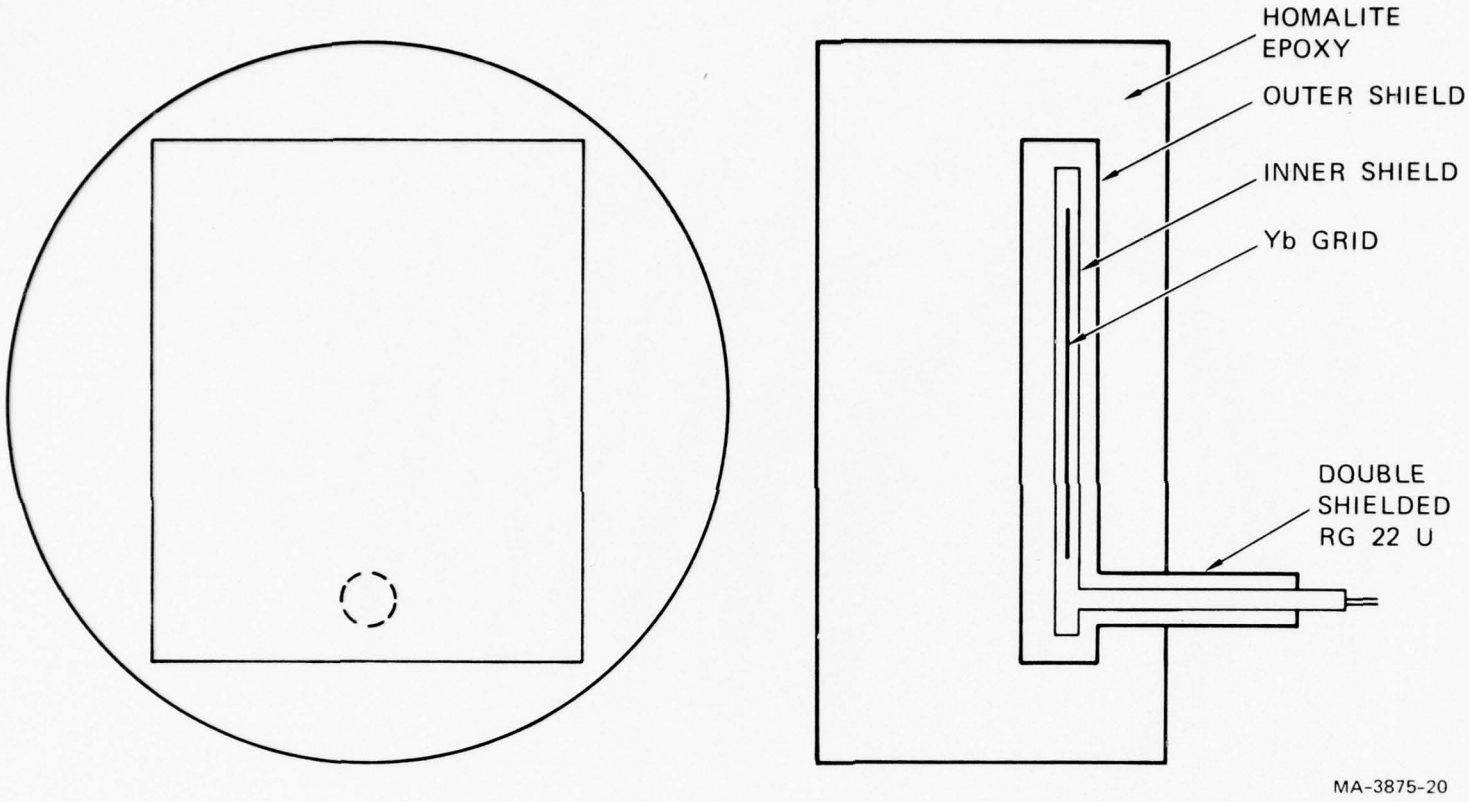

FIGURE A-1 DOUBLE SHIELDED EPOXY-YTTERBIUM GAGE

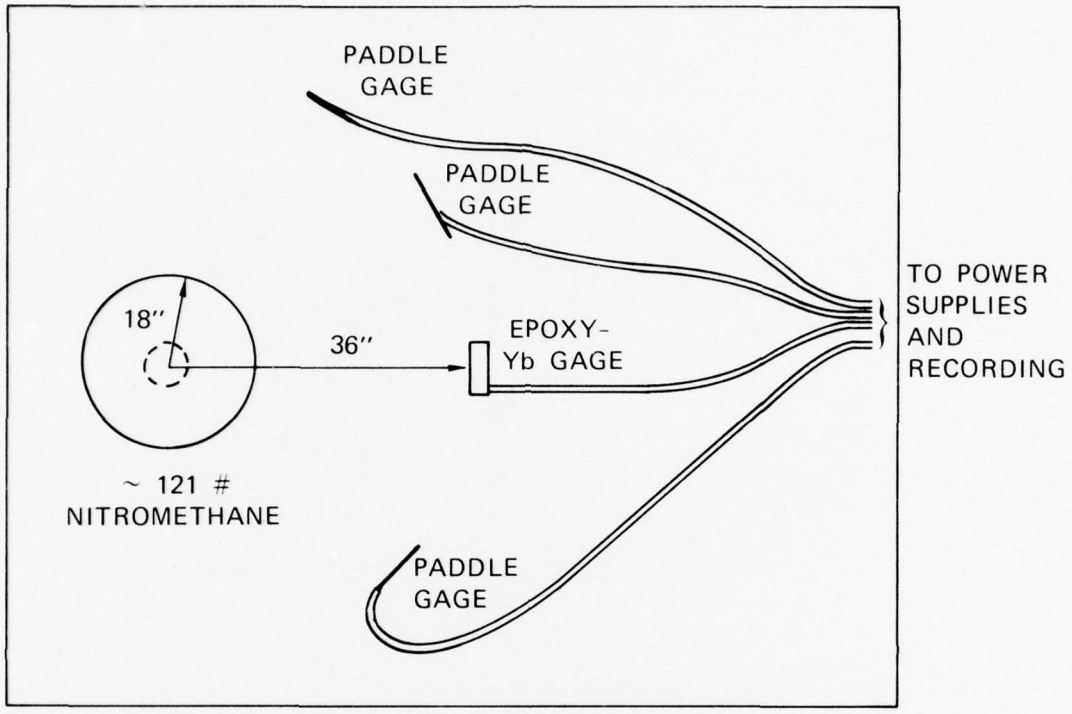

(a) PLAN VIEW

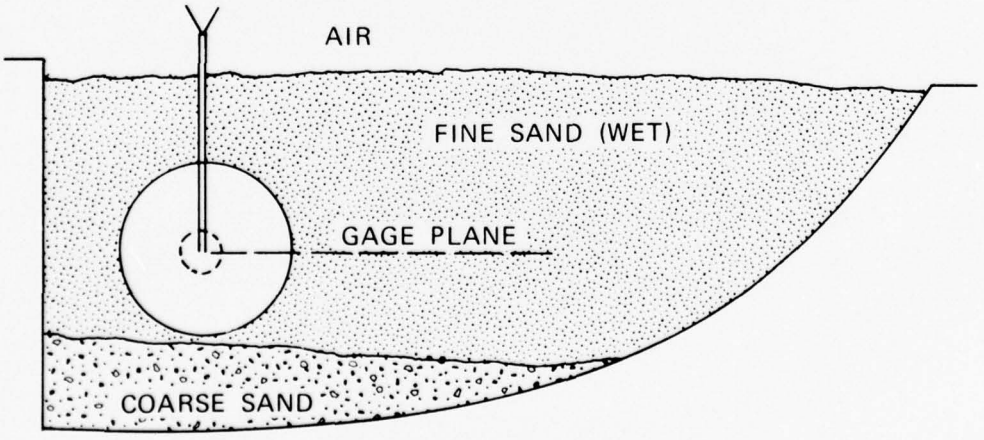

(b) ELEVATION

MA-3875-21

FIGURE A-2 HIGH EXPLOSIVE TEST CONFIGURATION

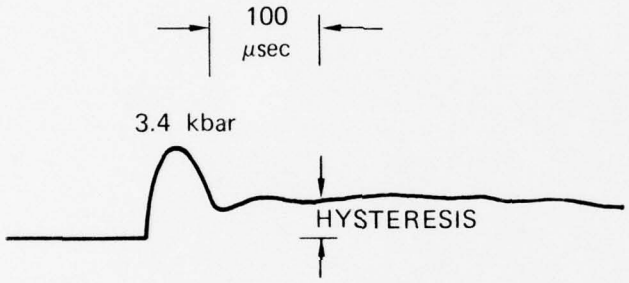

(a) EPOXY GAGE RECORD

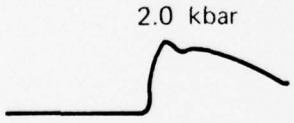

(b) TYPICAL PADDLE GAGE RECORD

MA-3875-22

FIGURE A-3 VOLTAGE-TIME PROFILES FOR HIGH EXPLOSIVE TEST

The results show two significant features: excellent recording duration was obtained by the block gage, and dissimilar wave shapes were recorded by the two types of gages. The recording duration is indicative that the complex, shielded joints of the block gage are adequately designed and constructed (Epoxy cylindrical gages typically do not fail as rapidly as the paddle gage). The dissimilar wave shape and peak stresses were of concern and necessitated the analysis described here.

1. Peak Stress

To explain the difference in peak stress measurement, it is instructive to look at shock wave data on saturated and partially saturated Ottawa banding sand obtained by Froula.[A-1]

The pertinent data are shown in Figures A-4 and A-5 (from Reference A-1). Note that plexiglas is a good impedance match to 100% saturated sand up to ~5 kbar. However, the impedance match diverges as the degree of saturation decreases. In Figure A-6, the C-7 data of Keough[1] are plotted. If homalite is assumed to be similar to C-7, the data can be used in a simple graphical analysis. Using the value of 2.1 kbar (determined by the paddle gages) as the equilibrium stress value in the sand and using the Froula Hugoniot for 23% saturation, a stress of ~2.9 kbar would be predicted in a block of C-7 (or Homalite). The gage in the Homalite would record this stress. The stress actually measured by the gage in Homalite was ~3.4 kbar. Clearly, if the saturation of the sand were slightly greater than 23%, the result of the graphical analysis would be close to the measured stress value.

It seems reasonable that the difference in peak stress recorded by the paddle gages and the block gage is caused by an impedance mismatch between the wet sand and the Homalite block, the sand being less than 100% saturated in the experiment at CHES. Total saturation would be difficult to achieve unless a liner (plastic) were placed between the sand and the dirt. Even then, the water would tend to be unevenly distributed.

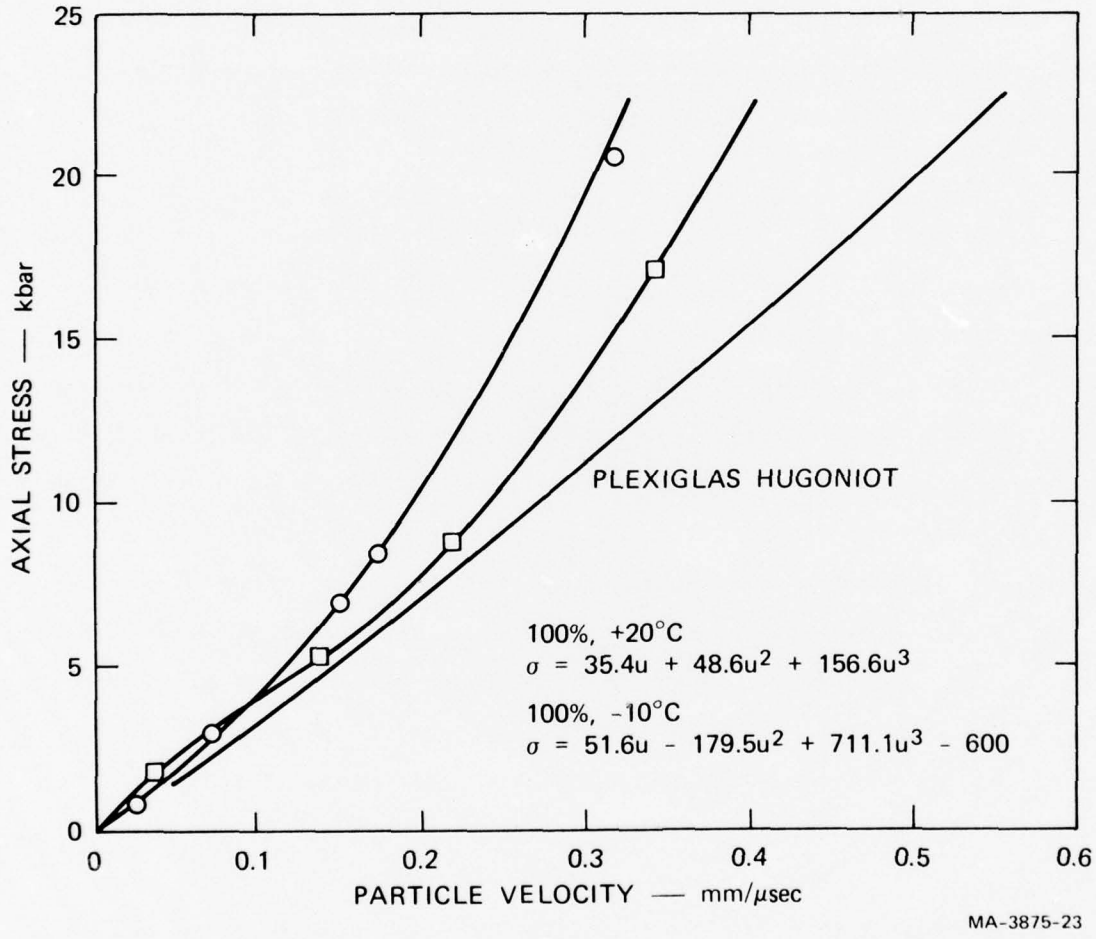

FIGURE A-4 STRESS VERSUS PARTICLE VELOCITY FOR OTTAWA BANDING SAND, 100% SATURATION, +20° AND -10°C (FROM FROULA, 1971)

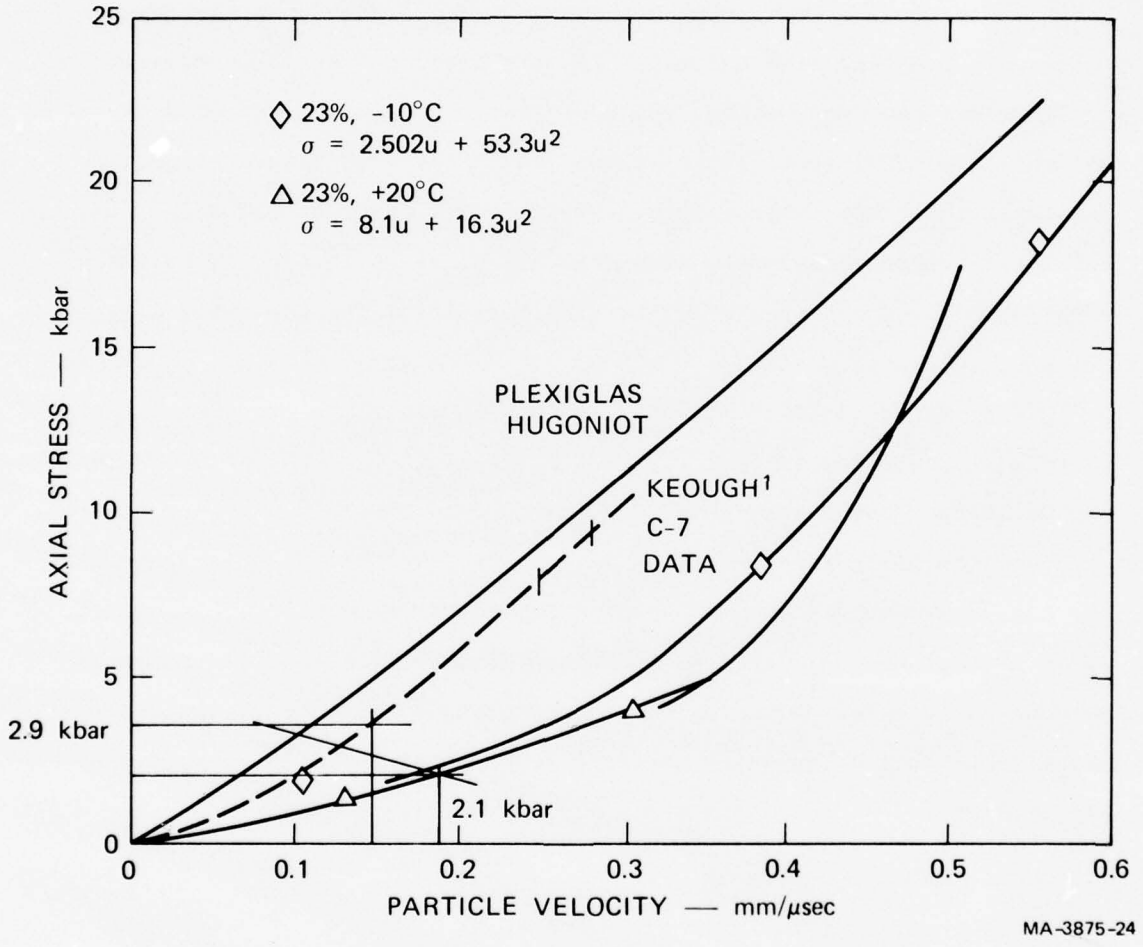

FIGURE A-5 STRESS VERSUS PARTICLE VELOCITY FOR OTTAWA BANDING SAND, 23% SATURATION, +20° AND -10°C (FROM FROULA, 1971)

2. Stress-Time Histories

The two major differences in profiles are the rapid decrease after peak and steady offset of the block gage compared to the expected exponential decay measured by the paddle gage.

It is reasonable to expect the more rapid decrease if the impedance mismatch cited above is assumed. In this case, relief waves from the cylindrical boundary between the epoxy and sand would occur between 10 and 14 μsec after first arrival of the longitudinal wave at the plane of the grid. In addition, a relief from the rear boundary will arrive at approximately the same time. A decrease comparable to the rise time would be expected after this because of the generally slow rise of the applied stress.

The rather constant offset after stress relief is somewhat larger than would be expected from residual resistance (hysteresis) as determined by Ginsberg.[4] At 3 kbar peak, Ginsberg's data show a hysteresis of ~26%, whereas the block gage indicates 32% to 37%. The higher percentage may be due to stretching caused by the lateral unloading waves. To obtain a more quantitative correlation between observed and expected profiles, a code calculation of the expected stress and strain states would be required. This calculation was felt to be unwarranted in view of the limited data from this test and complexity of the calculation.

3. Conclusion

The results of the high explosive tests indicated that the jointing of the shielded gage did not adversely affect longevity; the wave profiles, although different, were explainable and not due to the shielded grid configuration; and, finally, that the peak stress was as could be expected from the sand environment. Therefore, the double shielded grid is an adequate configuration for a soil stress gage.

Appendix B

STRESS-RESISTANCE CALIBRATION OF YTTERBIUM GAGE AT LOW STRESSES

1. Loading

All commonly used "stress" gages rely on a measurement of the state of strain within the gage. Applied loads that change the strain tensor in the transducing element therefore change the gage calibration. Ytterbium exhibits this behavior, as evidenced by the difference between the hydrostatic pressure and uniaxial strain coefficients of piezoresistance; $\sim 0.06\ \Omega/\Omega$ kbar and $0.04\ \Omega/\Omega$ kbar at 1 kbar, respectively. Since the gage matrix material will also affect the state of strain in the sensor, calibration should be performed in the matrix and mode of compression expected.

We examine here the data of Ginsberg,[4] Smith, et al.,[3] and Smith, et al.,[5] which reflect various loading curves for a variety of strain conditions. To date, calibrations have been performed in Lucite at high strain rates and uniaxial strain (shock) and in fiberglass (field configuration) at very low strain rates and essentially unknown strains (static). The different loading calibration curves in the low kilobar range are shown in Figure B-1.

The "unconfined" foil calibration was performed under uniaxial stress loading using Lucite platens,[3] i.e., the foil was not supported laterally. It is possible that the inflection in the curve is caused by yielding in the platens, which results in a large strain coupled to the foil and thus alters the resistance. The magnitude of the stress at the inflection point is consistent with the yield stress of plastics,

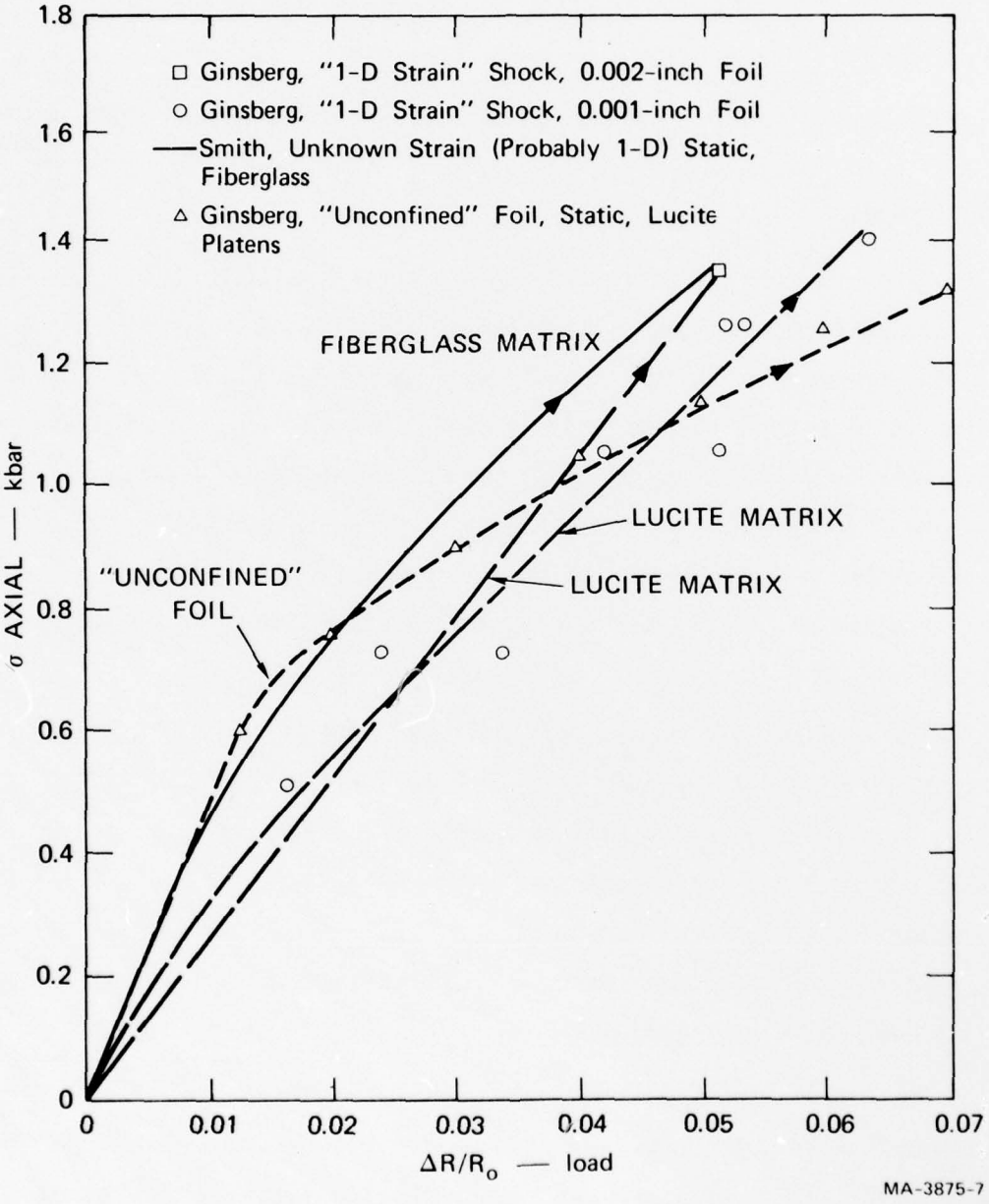

FIGURE B-1 LOW STRESS LOADING DATA

$\sim$0.8 kbar. The difficulty in using any of these calibrations to reduce field data is that the mode of compression in the field is not well known. The limits, however, probably fall within the uniaxial strain (Lucite) and the fiberglass. The fiberglass represents unconfined compression of the fiberglass and ytterbium package. More precise pressure calibration requires additional compression tests in which the strain states are carefully controlled. However, the uniaxial strain shock calibration appears to be accurate for reduction of field data to within $\sim \pm 15\%$.

2. Unloading

Calibration data for unloading response are shown in Figure B-2. Here the data have been normalized to a common $\Delta R/R_o$ peak value, i.e., resistance changes refer to the unload $\Delta R/R_o$. Again, the strain state is seen to affect the calibration, but to a lesser extent in the "expected" modes of compression, i.e., in the Lucite and fiberglass matrices. Here the "error" would be significantly less, a few percent maximum for the majority of the unloading data.

Multiple cycle unloading data exist for the fiberglass matrix tests.[3] These are shown in Figure B-3, together with the "unconfined" foil tests. These latter data illustrate the influence of the mode but are unrealistic with respect to gage use. It can be seen that the fiberglass matrix tends to load and unload with decreasing "hysteresis."

3. Reloading

Reloading data are shown in Figure B-4. Here the data show a greater dependence on foil thickness than on mode of compression. The curves marked "fiberglass matrix" and "Lucite matrix" represent data for one foil thickness, 0.002 inches. It is seen that the maximum difference again is on the order of $\pm 15\%$.

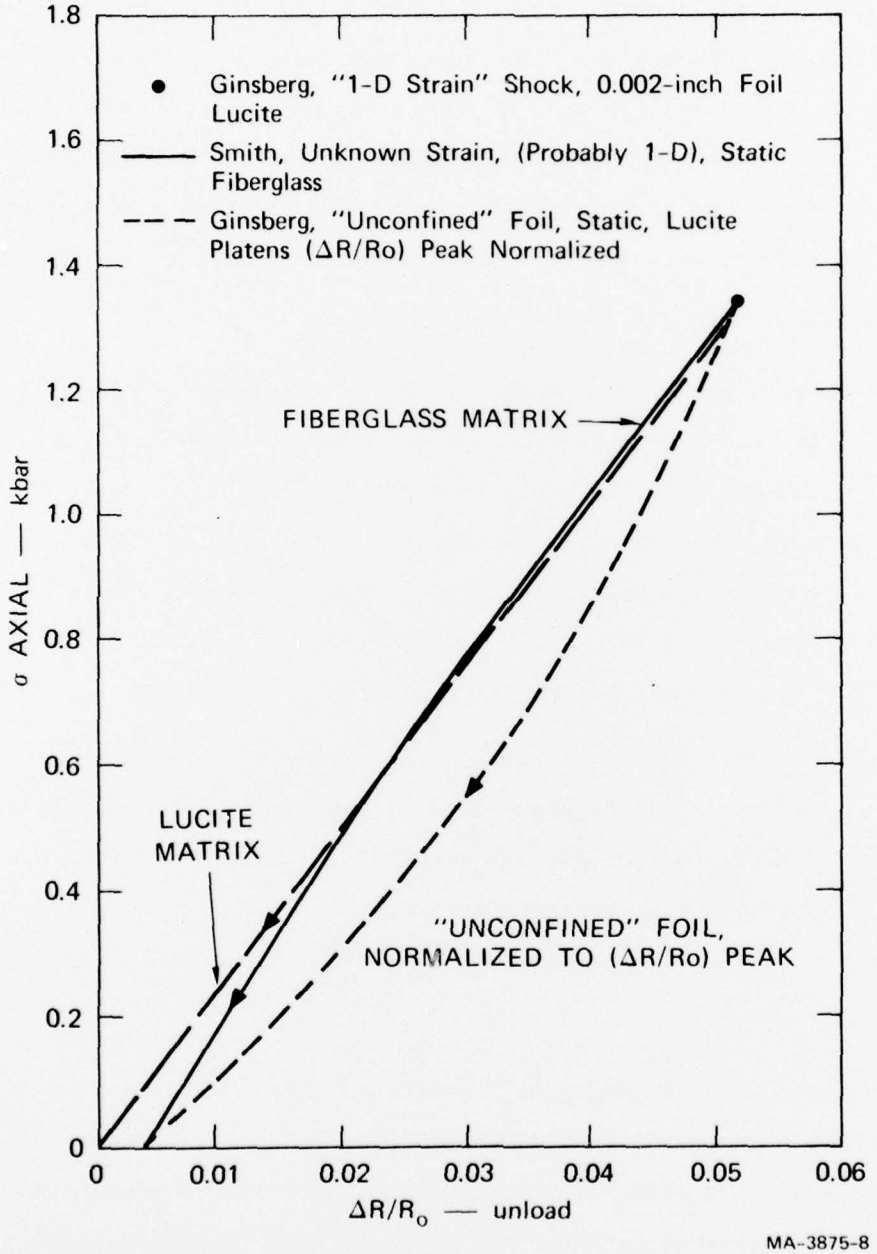

FIGURE B-2 LOW STRESS UNLOADING DATA

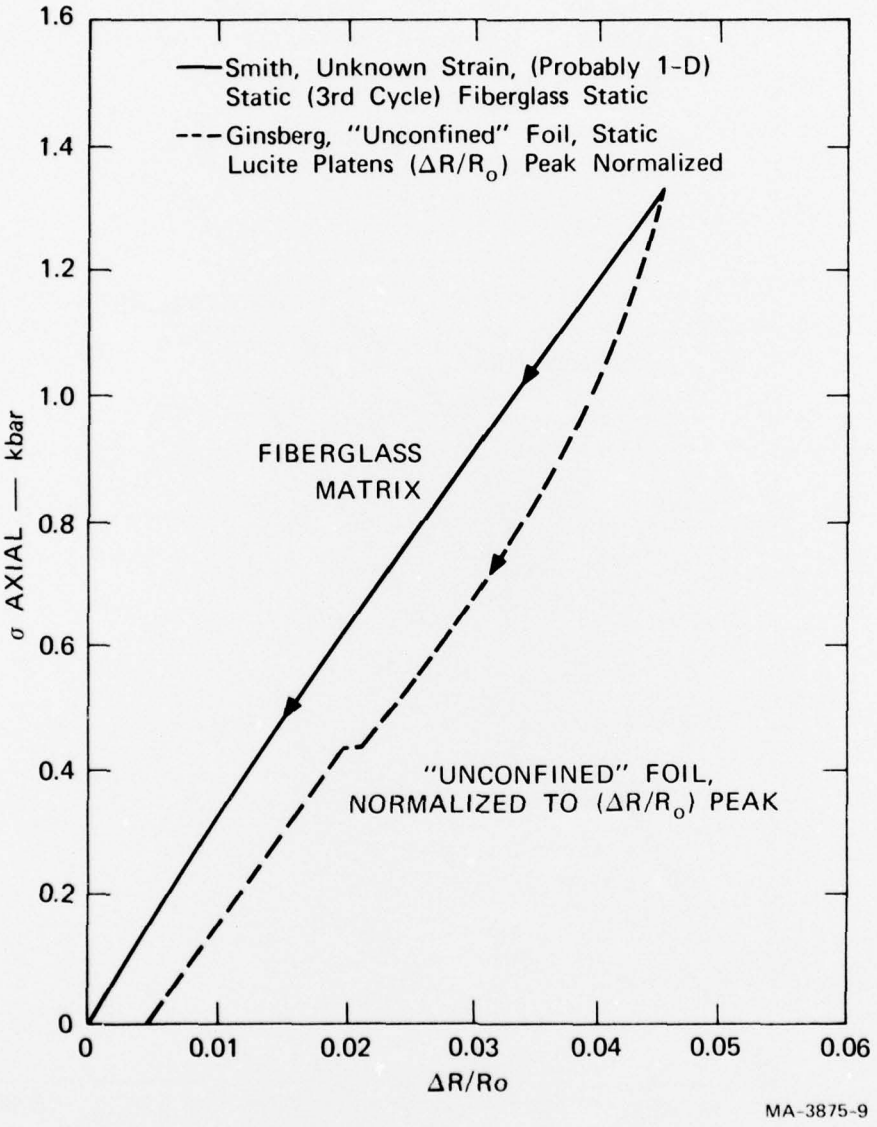

FIGURE B-3 LOW STRESS MULTIPLE CYCLE UNLOADING DATA

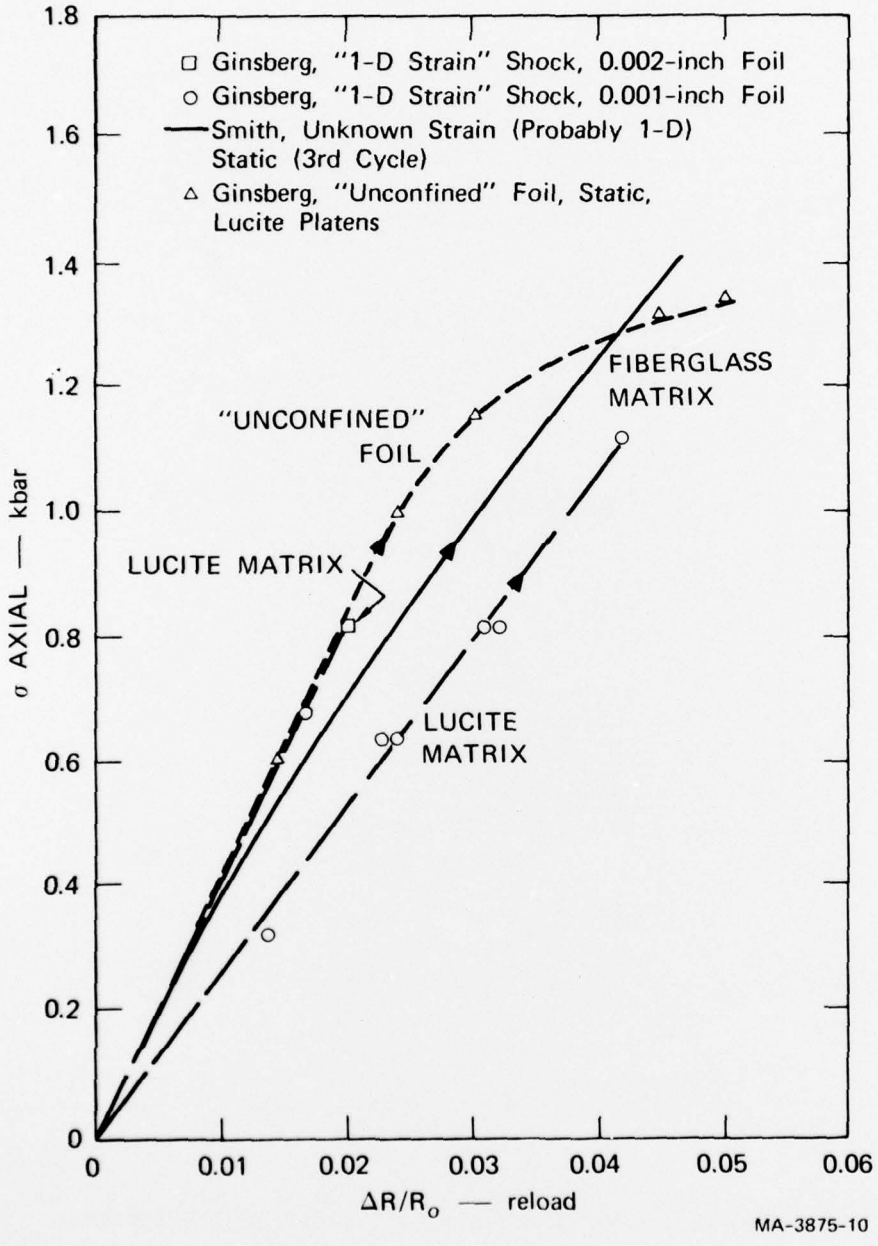

FIGURE B-4 LOW STRESS RELOAD DATA

4. Lower Stress Limit

The lower practical limit of stress sensitivity is somewhat a function of duration of the stress pulse being measured and the power supply system. As the duration increases, joule heating of the gage (due to the large viewing currents necessary to detect the resistance change) in a pulsed supply causes larger changes in resistance than do stresses. For short durations, a few hundred microseconds, a lower limit of tens of bars is practical. By use of ac bridges, rather than pulsed dc, a resolution of $\sim$ 100 bars has been obtained for durations of tens of milliseconds.

Appendix C

ESTIMATE OF UNDERREGISTRATION OF PRESSURE, LOW MODULUS GROUT IN HIGH MODULUS SOIL (ROCK)

The uncertainties discussed in Appendix B refer to stress in the gage matrix. Relating this stress to that in a surrounding medium is more difficult since the dynamic constitutive properties of the medium are often unknown. General studies of the response of various gages in the elastic range of gage and medium materials have shown strong dependence of gage stress on relative moduli, as well as on gage aspect ratio and on sensor-to-gage area. These studies have not been extended to the elastic-plastic regime. At stresses well above yield strengths, deviatoric stresses become less significant and gage stress can be readily related to medium stress. In this appendix, we estimate the possible effect of a mismatch in moduli between the gage-grout considered as a gage and the surrounding modium. In the case of tuff, we have assumed that the "gage" registers correctly because the grout is matched in modulus and strength to the tuff. This is not necessarily so, because the dynamic strengths in situ are largely unknown.

With respect to granite, an estimate can be made by considering the analysis for elastic material behavior as presented by Taylor[C-1] and others.

Taylor has shown that the relative pressure, gage to soil, is a function of the gage geometry and relative compressive moduli according to:

$$\frac{Pg - Ps}{Ps} = \left[\frac{K \quad 1 - \frac{Ms}{Mg}}{1 + \frac{B}{D} \cdot \frac{Ms}{Mg} \cdot K} \right] \cdot \frac{B}{D}$$

where Ps = soil pressure

Pg = gage pressure

K = constant

Ms = bulk modulus of soil

Mg = bulk modulus of gage

B = half thickness of gage

D = gage diameter .

If we assume the grout column to be our "gage," then B/D = 0.5 and the relative pressure, Pg/Ps, as a function of modulus ratio, Ms/Mg, is as shown in Figure C-1, where K has been assumed equal to 1.

In the case of a grout column in granite and in a stress range from $\sim$ 0.25 to 3 kbar:

Ms = constant $\simeq 10^{12}$ dynes/cm^2

Mg = 1×10^{11} to 2×10^{11} dynes/cm^2

and $\frac{Ms}{Mg}$ varies from 10 to 5.

The grout modulus is assumed to be identical to a nearly saturated ash-fall tuff. The "gage" underregisters from ~75% to 60% over the range from $\sim$ 0.25 kbar to $\sim$ 3 kbar granite pressure.

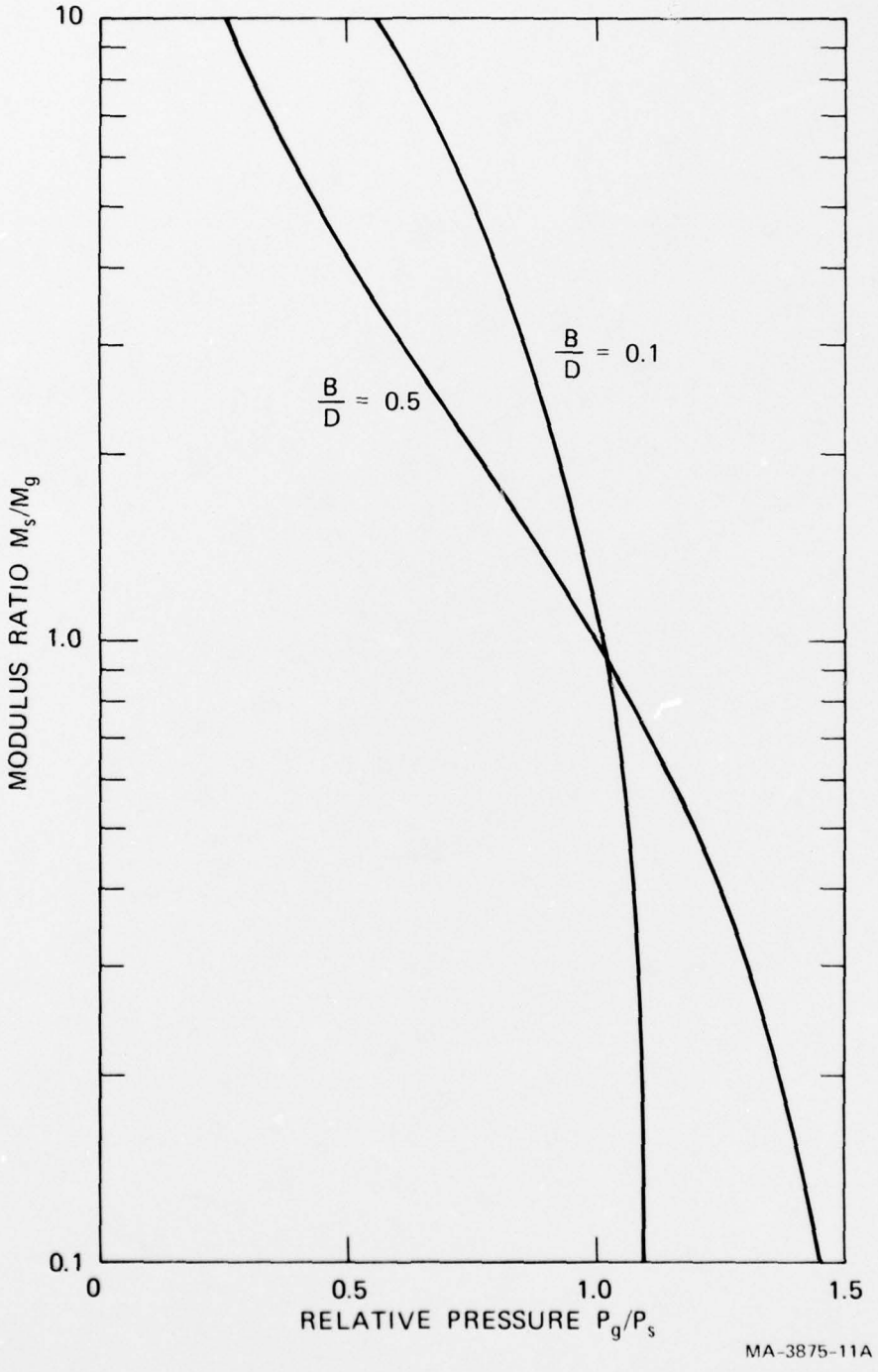

FIGURE C-1 RELATIVE PRESSURE AS A FUNCTION OF MODULUS RATIO

Appendix D

STRESS-RESISTANCE RESPONSE OF YTTERBIUM

0-10 kbar

The loading stress-resistance data for ytterbium have been fitted by Ginsberg[4] to the relations:

$$\sigma = 1.08^2 \quad 1 - \mathrm{Exp}(-20.80x) \quad + 9.108x$$

for

$x = \Delta R/R_o$ between 0.0 and

1.0 ($\sim$10 kbar).

Data for x in increments of 0.001 are given in Table D-1.

Table D-1

STRESS (σ) - RESISTANCE CALIBRATION DATA

DELTA R/R0	STRESS(KBAR)	DELTA R/R0	STRESS(KBAR)
0.000	0.0000000		
.001	.0314412	.051	1.1750026
.002	.0624238	.052	1.1918811
.003	.0929574	.053	1.2086609
.004	.1230512	.054	1.2251652
.005	.1527142	.055	1.2415772
.006	.1819554	.056	1.2578402
.007	.2107833	.057	1.2739571
.008	.2392065	.058	1.2899309
.009	.2672334	.059	1.3057647
.010	.2948720	.060	1.3214612
.011	.3221304	.061	1.3370233
.012	.3490164	.062	1.3524539
.013	.3755377	.063	1.3677555
.014	.4017018	.064	1.3829308
.015	.4275160	.065	1.3979825
.016	.4529875	.066	1.4129130
.017	.4781235	.067	1.4277250
.018	.5029307	.068	1.4424207
.019	.5274160	.069	1.4570027
.020	.5515859	.070	1.4714732
.021	.5754471	.071	1.4858346
.022	.5990058	.072	1.5000890
.023	.6222683	.073	1.5142388
.024	.6452406	.074	1.5282860
.025	.6679288	.075	1.5422328
.026	.6903386	.076	1.5560812
.027	.7124759	.077	1.5698332
.028	.7343462	.078	1.5834909
.029	.7559550	.079	1.5970562
.030	.7773077	.080	1.6105309
.031	.7984096	.081	1.6239170
.032	.8192658	.082	1.6372162
.033	.8398814	.083	1.6504305
.034	.8602614	.084	1.6635614
.035	.8804106	.085	1.6766107
.036	.9003337	.086	1.6895802
.037	.9200354	.087	1.7024714
.038	.9395203	.088	1.7152859
.039	.9587928	.089	1.7280254
.040	.9778573	.090	1.7406914
.041	.9967181	.091	1.7532853
.042	1.0153794	.092	1.7658088
.043	1.0338452	.093	1.7782632
.044	1.0521197	.094	1.7906499
.045	1.0702067	.095	1.8029703
.046	1.0881100	.096	1.8152259
.047	1.1058336	.097	1.8274179
.048	1.1233811	.098	1.8395476
.049	1.1407560	.099	1.8516164
.050	1.1579620	.100	1.8636255

Table D-1 (Concluded)

DELTA R/R0	STRESS(KBAR)	DELTA R/R0	STRESS(KBAR)
0.110	1.9806903		
.120	2.0929881	.510	5.7576533
.130	2.2014139	.520	5.8493383
.140	2.3066950	.530	5.9410224
.150	2.4094219	.540	6.0327057
.160	2.5100743	.550	6.1243884
.170	2.6090418	.560	6.2160705
.180	2.7066407	.570	6.3077523
.190	2.8031280	.580	6.3994338
.200	2.8987126	.590	6.4911149
.210	2.9935640	.600	6.5827959
.220	3.0878197	.610	6.6744767
.230	3.1815918	.620	6.7661573
.240	3.2749710	.630	6.8578379
.250	3.3680311	.640	6.9495182
.260	3.4608320	.650	7.0411985
.270	3.5534224	.660	7.1328788
.280	3.6458419	.670	7.2245590
.290	3.7381225	.680	7.3162392
.300	3.8302903	.690	7.4079194
.310	3.9223665	.700	7.4995995
.320	4.0143682	.710	7.5912796
.330	4.1063096	.720	7.6829597
.340	4.1982019	.730	7.7746397
.350	4.2900543	.740	7.8663198
.360	4.3818743	.750	7.9579998
.370	4.4736681	.760	8.0496799
.380	4.5654405	.770	8.1413599
.390	4.6571955	.780	8.2330399
.400	4.7489364	.790	8.3247199
.410	4.8406659	.800	8.4163999
.420	4.9323861	.810	8.5080799
.430	5.0240988	.820	8.5997600
.440	5.1158053	.830	8.6914400
.450	5.2075068	.840	8.7831200
.460	5.2992043	.850	8.8748000
.470	5.3908985	.860	8.9664800
.480	5.4825901	.870	9.0581600
.490	5.5742795	.880	9.1498400
.500	5.6659671	.890	9.2415200
		.900	9.3332000
		.910	9.4248800
		.920	9.5165600
		.930	9.6082400
		.940	9.6999200
		.950	9.7916000
		.960	9.8832800
		.970	9.9749600
		.980	10.0666400
		.990	10.1583200
		1.000	10.2500000

DISTRIBUTION LIST

DEPARTMENT OF DEFENSE

Director
Defense Advanced Rsch. Proj. Agency
ATTN: NMRO
ATTN: PMO
ATTN: STO

Director
Defense Communications Agency
ATTN: Code 930

Defense Documentation Center
12cy ATTN: TC

Director
Defense Intelligence Agency
ATTN: DB-4C2, Timothy Ross

Director
Defense Nuclear Agency
ATTN: STSI Archives
ATTN: DDST
2cy ATTN: SPTD
3cy ATTN: SPSS
3cy ATTN: STTL, Tech. Library

Dir. of Defense Rsch. & Engineering
ATTN: S&SS(OS)

Commander
Field Command, DNA
ATTN: FCTMD
ATTN: FCPR
2cy ATTN: FCTMOF
4cy ATTN: FCTMC

Chief
Livermore Division, Fld. Command DNA
ATTN: FCPRL

Chief
Test Construction Division
Field Command Test Directorate, DNA
2cy ATTN: FCTC

DEPARTMENT OF THE ARMY

Director
BMD Advanced Tech. Ctr.
ATTN: 1CRDABH-X
ATTN: CRDABH-S
ATTN: ATC-T, Melvin T. Capps

Program Manager
BMD Program Office
ATTN: DACF-BMT
ATTN: CRDABM-NE

Commander
BMD System Command
ATTN: BDMSC-TEN, Noah J. Hurst
ATTN: R. DeKalb

Dep. Chief of Staff For Rsch. Dev. & ACQ.
ATTN: DAMA-CSM-N

DEPARTMENT OF THE ARMY (Continued)

Chief of Engineers
ATTN: DAEN-MCE-D
ATTN: DAEN-RDM

Commander
Harry Diamond Laboratories
ATTN: DRXDO-TI, Tech. Lib.
ATTN: DRXDO-RBH, James H. Gwaltney
ATTN: A. J. Baba
ATTN: DRXDO-NP

Commander
Picatinny Arsenal
ATTN: SMUPA-ND-W

Director
U.S. Army Ballistic Research Labs
ATTN: Tech. Lib., Edward Baicy

Commander
U.S. Army Engineer Center
ATTN: ATSEN-SY-L

Division Engineer
U.S. Army Engineer Div. Huntsville
ATTN: HNDED-SR

Director
U.S. Army Engr. Waterways Exper. Sta.
ATTN: J. D. Day
ATTN: James Ballard
ATTN: Guy Jackson
ATTN: John N. Strange
ATTN: William Flathau
ATTN: J. K. Ingram

Commander
U.S. Army Nuclear Agency
ATTN: Tech. Lib.

DEPARTMENT OF THE NAVY

Officer-In-Charge
Civil Engineering Laboratory
Naval Construction Battalion Center
ATTN: Stan Takahashi
ATTN: Technical Library
ATTN: R. J. O' Dello
ATTN: J. Crawford
ATTN: L51, Warren Shaw

Commander
Naval Facilities Engineering Command
Headquarters
ATTN: Technical Library

Naval Plant Representative
Naval Plant Representative Office
Strategic Systems Project Office
Lockheed Missile and Space Company
ATTN: SPL 325

DEPARTMENT OF THE NAVY (Continued)

Director
Naval Research Laboratory
ATTN: Code 2600, Tech. Lib.

Commander
Naval Surface Weapons Center
ATTN: Kurt Inkenhaus
ATTN: WA50

DEPARTMENT OF THE AIR FORCE

AF Weapons Laboratory, AFSC
ATTN: RN(NT)
ATTN: DES-S, M.A. Plamondon
ATTN: DEP, Jimmie L. Bratton
ATTN: DED
ATTN: *DES-C, Robert Henny*
ATTN: SUL
ATTN: DES-G, Mr. Melzer
ATTN: RNB(NS)
ATTN: RNE(EL)
2cy ATTN: RND(DY)

Headquarters
Air Force Systems Command
ATTN: Technical Library

Commander
Foreign Technology Division, AFSC
ATTN: TD-BTA, Library

HQ USAF/RD
ATTN: RDQSM

SAMSO/DE
ATTN: DEB

ENERGY RESEARCH & DEVELOPMENT ADMINISTRATION

University of California
Lawrence Livermore Laboratory
ATTN: David Oakley, L-21
ATTN: Victor Karpenko, L-113

Los Alamos Scientific Laboratory
ATTN: Doc. Control for Reports Lib.

Sandia Laboratories
Livermore Laboratory
ATTN: Doc. Control for Tech. Library

Sandia Laboratories
ATTN: Doc. Con. for Wendell D. Weart
ATTN: Doc. Con. for Luke J. Vortman
ATTN: Doc. Con. for 3141, Sandia Rpt. Coll.
ATTN: Doc. Control for Carter Broyles

OTHER GOVERNMENT AGENCIES

Department of the Interior
U.S. Geological Survey
Special Projects Center
ATTN: William Twenhofel
ATTN: Arthur Fernald

OTHER GOVERNMENT AGENCIES (Continued)

Department of the Interior
U.S. Geological Survey
ATTN: Cecil B. Raleigh
ATTN: J. H. Healy

DEPARTMENT OF DEFENSE CONTRACTORS

Aerospace Corporation
2cy ATTN: Tech. Info. Services

Agbabian Associates
ATTN: Carl Bagge
ATTN: M. Agbabian

Analytic Services, Inc.
ATTN: George Hesselbacher

Applied Theory, Inc.
2cy ATTN: John G. Trulio

Artec Associates, Inc.
ATTN: Steven Gill

Battelle Memorial Institute
ATTN: Technical Library

The BDM Corporation
ATTN: Tech. Lib.

The Boeing Company
ATTN: *Robert Dyrdahl*
ATTN: Aerospace Library

Brown Engineering Company, Inc.
ATTN: Manu Patel

California Research & Technology, Inc.
ATTN: Sheldon Shuster
ATTN: Ken Kreyenhagen
ATTN: Technical Library

Civil/Nuclear Systems Corp.
ATTN: Robert Crawford

Electromechanical Sys. of New Mexico, Inc.
ATTN: R. A. Shunk

Engrg. Decision Analysis Co., Inc.
ATTN: R. P. Kennedy

General Electric Company
TEMPO-Center for Advanced Studies
ATTN: DASIAC

H-Tech Laboratories
ATTN: B. Hartenbaum

IIT Research Institute
ATTN: Technical Library

Institute for Defense Analyses
ATTN: IDA Librarian, Ruth S. Smith

J. H. Wiggins Co., Inc.
ATTN: John Collins

DEPARTMENT OF DEFENSE CONTRACTORS (Continued)

Kaman Sciences Corporation
ATTN: Frank H. Shelton

Lockheed Missiles & Space Co., Inc.
ATTN: Jack Wilson, Dept. 58-10
ATTN: A. Risso, Dept. 58-10, Bld. 102
ATTN: Edwin A. Smith, Dept. 85-85

Lockheed Missiles and Space Company
ATTN: S. R. Salisbury
ATTN: Tom Geers
ATTN: Lloyd F. Chase

McDonnell Douglas Corporation
ATTN: J. Kirby
ATTN: H. M. Berkowitz

Merritt Cases, Incorporated
ATTN: Technical Library
ATTN: J. L. Merritt

Mission Research Corporation
ATTN: Conrad L. Longmire

Mission Research Corporation
ATTN: David E. Merewether

Mission Research Corporation-San Diego
ATTN: V. A. J. Van Lint

The Mitre Corporation
ATTN: Library

University of New Mexico
Dept. of Campus Security and Police
ATTN: G. E. Triandafalidis

Newmark, Nathan M.
Consulting Engineering Services
University of Illinois
ATTN: W. Hall
ATTN: Nathan M. Newmark

Pacifica Technology
ATTN: R. Bjork
ATTN: G. Kent

Physics International Company
ATTN: Doc. Control for Dennis Orphal
ATTN: Doc. Con. for Charles Godfrey
ATTN: Doc. Con. for Fred M. Sauer
ATTN: Doc. Control for Coye Vincent
ATTN: Joe Kochley
ATTN: Doc. Con. for Larry A. Behrmann

DEPARTMENT OF DEFENSE CONTRACTORS (Continued)

The Rand Corporation
ATTN: Technical Library

R & D Associates
ATTN: Henry Cooper
ATTN: Technical Library
ATTN: J. G. Lewis
ATTN: Robert Port
ATTN: Cyrus P. Knowles
ATTN: Harold L. Brode

Science Applications, Inc.
ATTN: R. Parkinson
ATTN: Larry Scott
ATTN: Olan Nance

Science Applications, Inc.
ATTN: R. I. Miller

Science Applications, Inc.
ATTN: James Cramer
ATTN: J. Roger Hill

Sciences Applications, Incorporated
ATTN: Burt Chambers

Stanford Research Institute
ATTN: H. E. Lindberg
ATTN: George Carpenter
ATTN: George R. Abrahamson
ATTN: Douglas D. Keough
ATTN: Donald R. Curran

Systems, Science and Software, Inc.
ATTN: Bud Pyatt
ATTN: Phil Coleman
ATTN: Technical Library
ATTN: Donald R. Grine
ATTN: Russell E. Duff
ATTN: Charles R. Dismukes

Terra Tek, Inc.
ATTN: Technical Library
ATTN: Sidney Green

TRW Systems Group
ATTN: Peter K. Dai, R1/2170
ATTN: Norm Lipner
ATTN: Tech. Info. Center/S-1930

TRW Systems Group
ATTN: Gregory D. Hulcher

Weidlinger Assoc. Consulting Engineers
ATTN: Melvin L. Baron